Ocean Engineering 361 (2026) 126169

Contents lists available at ScienceDirect

Ocean Engineering

journal homepage: www.elsevier.com/locate/oceaneng

Research paper

A novel hybrid physics-data driven encoder-decoder model for wind turbine wake predictions

Maokun Ye [a], Hanqiao Han [b], Minqiu Liu [a], Decheng Wan [a,*], Moustafa Abdel-Maksoud [c]

[a] Computational Marine Hydrodynamics Lab (CMHL), School of Ocean and Civil Engineering, Shanghai Jiao Tong University, Shanghai, China
[b] Wuhan Second Ship Design and Research Institute, Wuhan, China
[c] Hamburg University of Technology (TUHH), Institute for Fluid Dynamics and Ship Theory (M8), Hamburg, Germany

ARTICLE INFO

Keywords:
Wind turbine wake
Artificial neural networks
Light-weight attention mechanisms
Hybrid physics-data method

ABSTRACT

Fast and accurate monitoring or prediction of wind turbine wakes is essential for real-time optimization of wind farm power generation. However, conventional approaches face significant challenges: direct field measurements using instruments like LiDAR are often economically infeasible due to high costs, high-fidelity numerical simulations are computationally prohibitive and slow for real-time applications, and purely data-driven machine learning methods typically suffer from poor physical interpretability and uncontrolled errors in full-field predictions. To address these limitations, we propose *wakeEvoNet*, a novel hybrid physics-data driven framework for real-time wind turbine wake monitoring/prediction. This approach strategically deploys sparse but high-fidelity measurement points in the near-wake region (within 3 rotor diameters downstream) to capture flow velocity profiles, which are then used as input for convolutional neural network (CNN) based encoder-decoder models to infer the downstream wake field (from 4D to 14D downstream). By feeding real-time monitored data at each time step, the model prevents temporal error accumulation common in sequential predictions. This hybrid methodology—combining direct measurements in the near-wake with neural network-based evolution for the far-wake—significantly reduces the number of required instruments while maintaining high accuracy across the entire wake field. In this study, we demonstrate the framework using the NREL 5 MW reference turbine under neutral atmospheric boundary layer conditions. High-fidelity computational fluid dynamics simulations employing large eddy simulation and the actuator line method are leveraged to generate the training datasets, and three convolutional neural network-based encoder-decoder architectures are developed: a benchmark U-Net (*wakeEvoNet*-1), a CBAM-enhanced U-Net (*wakeEvoNet*-2), and a novel CA-TA-UNet (*wakeEvoNet*-3) incorporating a physics-guided lightweight spatial attention mechanism tailored for wind turbine wake flows. The models utilize three consecutive upstream cross-sections to predict subsequent downstream fields, with results showing high accuracy (R^2 scores consistently above 0.80) and robust temporal performance on test data, offering an efficient alternative to traditional methods for real-time wind turbine wake monitoring/prediction.

1. Introduction

Wind power is projected to supply approximately one-third of the global electricity demand by 2050 (Veers et al., 2019), necessitating a several-fold increase in wind energy generation from current levels to realize this potential. Consequently, the efficient development of wind energy is paramount for the global energy transition. A pivotal challenge in wind farm operations arises from wake effects: downstream turbines operate within the wakes generated by upstream turbines, encountering reduced mean wind speeds and heightened velocity fluctuations compared to the undisturbed flow (Porté-Agel et al., 2020). This phenomenon not only substantially diminishes the power generation efficiency of downstream turbines but also significantly complicates the prediction of their power output (Abkar and Porté-Agel, 2014), (Archer et al., 2018), with empirical data indicating that total power losses due to wake effects in large wind farms typically range between 10% and 25% (Nilsson et al., 2015). Therefore, real-time monitoring and prediction of wind turbine wake fields are critically important for enabling dynamic optimization of wind farm power control, as they facilitate immediate adjustments to turbine operations, mitigate cumulative losses, and enhance overall energy yield. Consequently, developing accurate and efficient methods for monitoring or predicting wind-turbine

* Corresponding author.
E-mail address: dcwan@sjtu.edu.cn (D. Wan).

https://doi.org/10.1016/j.oceaneng.2026.126169
Received 17 December 2025; Received in revised form 10 May 2026; Accepted 19 May 2026
Available online 23 May 2026
0029-8018/© 2026 Elsevier Ltd. All rights reserved, including those for text and data mining, AI training, and similar technologies.

wake fields is indispensable for maximizing the operational efficacy and economic returns of wind farms, thereby accelerating the sustainable utilization of wind resources (Shakoor et al., 2016).

Existing methodologies for wind turbine wake field monitoring and prediction can be broadly categorized into three groups: direct measurement, physics-based modeling—which includes analytical wake models and numerical simulations—and data-driven methods. Ideally, employing high-precision instrumentation for real-time, full-field direct measurement would be the most straightforward and accurate approach. Various tools such as meteorological towers and LiDAR have been deployed to monitor wind turbine wake fields. However, the high installation and maintenance costs of such equipment, particularly in complex terrains and harsh offshore environments, render widespread implementation economically unfeasible. Furthermore, data acquired through physical measurements are inherently sparse in space, which inadequately supports comprehensive real-time monitoring of entire wind farms (Xu et al., 2026). Consequently, physics-based wind turbine wake modeling approaches are commonly utilized to achieve full-field wind turbine wake predictions.

Existing mainstream physics-based wind turbine wake modeling approaches can be categorized into analytical wake models and numerical simulation methods (Ye et al., 2023a), both of which face inherent compromises between computational efficiency and prediction accuracy. Analytical wake models typically describe explicit spatial relationships for time-averaged physical quantities (e.g., wind velocity) within single-turbine wakes (Jensen, 1983), (Bastankhah and Porté-Agel, 2014), (Qian and Ishihara, 2018). Through superposition techniques, these models can be extended to predict multi-turbine wake fields. Their primary advantage lies in computational efficiency: by avoiding iterative solutions of large partial differential equation systems, analytical models enable rapid characterization of multi-turbine wake features. Consequently, they are widely adopted for power output predictions for fixed-bottom wind farms (Sun and Yang, 2018), (Shao et al., 2019), (Zong and Porté-Agel, 2020). However, a significant limitation emerges when applying these models to complex environment, e.g., they struggle to capture the three-dimensional, unsteady characteristics of floating turbine wake fields, severely compromising their predictive applicability in offshore environments (Tran et al., 2014), (Xu et al., 2023). On the other hand, computational fluid dynamics (CFD)-based numerical methods solve the three-dimensional governing flow equations - i.e. the Navier-Stokes equations - through an iterative manner to reproduce turbulent wake evolution. These simulations can incorporate turbine effects through either direct blade-resolved (Lynch and Smith, 2013), (Ye et al., 2023b) modeling or equivalent force representations, including Blade Element Method (BEM)-based techniques such as actuator disc (AD) (Mikkelsen, 2003), actuator line (AL) (Sørensen and Shen, 2002), (Shen et al., 2005), and actuator surface (AS) models (Shen et al., 2007), (Shen et al., 2009). This direct physical modeling capability gives CFD simulations an irreplaceable advantage in capturing near-field wake dynamics (Tran and Kim, 2015), (Tran and Kim, 2016), (Ye et al., 2024). Nevertheless, for far-field wake prediction, CFD's prohibitive computational costs severely constrain fast forecasting capabilities and large-scale dynamic wind farm monitoring/analyses. This persistent trade-off between accuracy and efficiency fundamentally restricts the practical engineering application of both approaches across different wind farm applications.

In recent years, data-driven, or machine learning, methods, particularly artificial neural networks (ANNs, or NNs), have demonstrated significant potential for fluid flow modeling by establishing nonlinear mappings between input parameters and output physical fields, enabling efficient prediction of complex spatiotemporal flow characteristics. For wind turbine wake prediction, representative studies include Ti et al. (2020), (Ti et al., 2021) who employed actuator disk-based CFD simulations to model fixed single-turbine wakes, establishing direct mappings between spatiotemporal coordinates (x, y, z, t) and wind velocity components (u, v, w) using multi-layer perceptron (MLP), later extending this framework to multi-turbine configurations through analytical wake superposition models. Similarly, Li et al. (Li, 2023) utilized graph neural networks (GNNs) to parameterize fixed single-turbine wake fields using inflow velocity and yaw angle as inputs to predict time-averaged steady-state wake profiles, subsequently applying quadratic wake superposition to analyze eight in-line turbines. While these studies focus on direct mappings between operational parameters and wake physics, solely relying on neural network (NN) models to simulate wind turbine wake fields presents two fundamental limitations that constrain their predictive capability and physical fidelity. First, NN models exhibit significant limitations in capturing near-wake physics. The near-wake region (within 1D - 3D downstream) involves complex, multi-scale flow phenomena such as tip vortex interactions with tower structures and ambient turbulence. These intricate aerodynamic features stem directly from blade-induced flow separation and pressure gradients, which data-driven models struggle to resolve without explicit physical constraints(Li et al., 2022), (Yang et al., 2022), (Li et al., 2023), (Li et al., 2024). However, attempting direct NN-based near-wake modeling necessitates exponentially expanding the parameter space for training data generation. Consequently, the computational resources required to produce high-fidelity measurement or CFD datasets for training would increase prohibitively, ultimately diminishing any computational efficiency advantage over direct measurement or CFD simulation. Although recent studies (Zhang and Zhao, 2023) have incorporated physical loss functions into Physics-Informed Neural Networks (PINNs) for near-wake modeling, these approaches still being struggle to resolve critical flow details essential for accurate wake predictions. More recently, machine learning methods have been increasingly applied to reconstruct full flow fields from physically acquired yet spatially sparse measurements, giving rise to the rapidly evolving physics-data hybrid modeling paradigm. For example, Luo et al. (2024) (Luo et al., 2024) developed a proper orthogonal decomposition (POD)-based reduced-order modeling (ROM) framework for wind turbine wake reconstruction: POD was first employed to decompose high-fidelity wake snapshots into orthogonal dominant modes and low-dimensional temporal coefficients, and a 5-layer Wake Flow Estimation (WFE) neural network was subsequently trained to establish the nonlinear mapping between sparse sensor readings and these coefficients, enabling accurate full wake field reconstruction via linear combination of precomputed modes and predicted coefficients. Ye et al. (2026) (Ye et al., 2026) proposed a weakly constrained physics-informed neural network (PINN) to reconstruct wind turbine wake fields from three cross-sectional measurement lines, demonstrating that embedding the mass conservation law into the neural network loss function significantly enhances reconstruction accuracy, particularly in capturing the skewed tower wake structure. Nevertheless, existing studies have predominantly limited their investigations to wake fields in the turbine-hub horizontal plane, while the vertical structure of wind turbine wakes—an equally critical component for comprehensive wake monitoring and wind farm operational optimization—remains understudied and warrants further exploration.

Based on the preceding analysis, it becomes evident that the three conventional approaches to wind turbine wake monitoring and prediction each possess significant limitations: (1) While direct measurement can accurately monitor real-time flow conditions, its deployment is typically sparse in practical applications due to cost constraints; (2) Physics-based modeling, particularly high-fidelity numerical simulation, can achieve high accuracy but is computationally prohibitive and unsuitable for real-time tasks; (3) Purely data-driven methods suffer from inherent drawbacks such as difficulties in modeling the complex near-wake physics, poor interpretability, and challenges in controlling full-field prediction errors. As an attempt to address these challenges comprehensively, we introduce *wakeEvoNet*—a novel hybrid physics-data framework designed for real-time wind turbine wake monitoring and prediction. Our approach strategically decomposes the spatial domain to leverage the complementary strengths of direct measurement and data-driven modeling. The framework operates on two distinct spatial regimes.

- a physics-driven near-field (1D - 3D downstream), where direct measurements capture the intricate flow features directly influenced by the rotating turbine blades
- a data-driven far-field (4D - 14D downstream), where neural network (NN) models evolve the wake development using the upstream flow field as input.

The primary objective of this hybrid framework is to preserve the accuracy of direct measurements in the critical near-wake region while enabling rapid, high-precision prediction of the far-wake development through NN models. The architecture employs convolutional encoder-decoder networks, enhanced with a physics-guided lightweight attention mechanism, to model the cross-sectional wake evolution. Specifically, the model utilizes three consecutive upstream cross-sectional planes to predict the subsequent downstream section. This strategic design allows for the concentration of a limited number of high-precision measurement instruments in the near-wake region (1D to 3D). The real-time data acquired from these points is then fed into the neural network, enabling the inference of the entire wake field information. Consequently, this methodology significantly reduces the required number of costly high-precision measurements while maintaining high accuracy in the prediction and monitoring of the complete wind turbine wake field.

The primary contributions and novelties of this work are two-folded.

1. Novel spatial-decomposition framework: we introduce *wakeEvoNet*, a hybrid physics-data framework that fundamentally reconfigures wake monitoring/prediction through spatial domain decomposition. Unlike conventional approaches applying neural networks to full-field prediction, our methodology anchors each prediction step in measured/monitored flow data of the near-wake region (1D - 3D downstream) while deploying specialized neural networks to evolve this physically-grounded initial condition into the far-field (4D - 14D downstream). This spatial partitioning is able to eliminate temporal error accumulation inherent in time-dependent prediction schemes (Deng et al., 2019), (Chen et al., 2021), (Cao et al., 2024), maintaining accuracy throughout extended monitoring by resetting error accumulation at each time step.
2. New physics-guided lightweight spatial attention: For wake cross-section prediction, we propose Turbine-wake Attention (TA) mechanism - a lightweight spatial attention module that dynamically weights features based on local velocity features which is designed for wind-turbine-wake prediction tasks. This innovation strategically amplifies local flow regions during wake evolution, outperforming conventional attention modules like CBAM's Spatial Attention by 3-15% R^2 across downstream distances in the current study.

The remainder of this paper is organized as follows: Section 2 details the test-case configuration, including the specifications of the NREL 5 MW reference wind turbine and the high-fidelity computational setup that combines Large Eddy Simulation (LES) with the Actuator Line Method (ALM) to generate the high-quality dataset essential for model training. Section 3 elaborates on the developed neural network architectures, beginning with the benchmark U-Net (*wakeEvoNet*-1) and progressively introducing the attention-enhanced models, *wakeEvoNet*-2 and *wakeEvoNet*-3, with a focused explanation of the novel physics-guided Turbine-wake Attention (TA) mechanism. Section 4 presents a comprehensive evaluation of the models, assessing their spatial accuracy, temporal consistency, and error characteristics under a rolling prediction scheme, and includes an interpretative analysis of the models' operational focus. Finally, Section 5 concludes the paper by summarizing the key findings, highlighting the framework's contributions and limitations, and suggesting avenues for future research.

2. Test-case description

2.1. The reference wind turbine

In the current study, the NREL 5 MW reference wind turbine is adopted, which a benchmark model in wind energy research. Key specifications of this wind turbine include: rated wind speed of 11.4 m/s, rated rotational speed of 12.1 rpm, rotor diameter of 126 m, and hub height of 90 m. Comprehensive technical details of this reference turbine are documented in the foundational technical report by Jonkman et al. (2009) and are omitted here for conciseness. The simulated inflow conditions correspond to a neutral atmospheric boundary layer (ABL) with mean wind speed matching the turbine's rated operational point at hub height (11.4 m/s).

2.2. Wind turbine wake simulation using Computational Fluid Dynamics (CFD) methods

In this study, high-fidelity numerical simulations are employed to generate datasets for validating the feasibility of the proposed hybrid physics-data driven framework. Computational fluid dynamics (CFD) is leveraged to simulate the wake field of a single NREL 5 MW reference wind turbine under neutral atmospheric boundary layer (ABL) conditions, thereby producing the essential dataset for training subsequent neural network (NN) models. This section elaborates on the numerical methodologies used for dataset generation, which encompass: (1) the governing fluid dynamics equations based on the large-eddy simulation (LES) approach; (2) the implementation of the actuator line method (ALM) for modeling rotating wind turbine blades; and (3) the two-stage precursor simulation procedure for generating realistic neutral ABL inflow conditions.

2.2.1. Governing equations

This study employs Large Eddy Simulation (LES) as the fundamental computational framework for high-fidelity wake field simulation. LES resolves turbulent flow physics through scale separation: large-scale turbulent structures are directly solved through numerical integration of the Navier-Stokes equations, while subgrid-scale turbulence is represented through a subgrid stress model. The spatial filter scale Δ is determined as the geometric mean of grid cell dimensions in three orthogonal directions, i.e. $\Delta = \left(\Delta_x \Delta_y \Delta_z\right)^{1/3}$, where Δ_x, Δ_y, and Δ_z represent grid cell sizes in the streamwise, cross-flow, and vertical directions, respectively. The filtered governing equations for incompressible flow incorporate essential physical influences including turbine aerodynamic forces, Coriolis effects from Earth's rotation, and thermal buoyancy effects, expressed as:

$$\frac{\partial \widetilde{u}_i}{\partial x_i} = 0 \tag{1}$$

$$\frac{\partial \overline{u}_i}{\partial t} + \frac{\partial\left(\overline{u}_j \overline{u}_i\right)}{\partial x_j} = -\frac{\partial \widehat{p}}{\partial x_i} - \frac{\partial \tau_{ij}^D}{\partial x_j} - \frac{1}{\rho_0}\frac{\partial \overline{p}_0(x,y)}{\partial x_i} + g\left(\frac{\overline{\theta}-\theta_0}{\theta_0}\right)\delta_{i3} - 2\varepsilon_{i3k}\Omega_3\overline{u}_k + \frac{F_i}{\rho_0} \tag{2}$$

where t denotes time; u_i represents velocity components ($i = 1,2,3$); $\widehat{p}$ is modified pressure; ρ_0 is reference air density; F_i denotes forces applied to the flow field by wind turbines; g is gravitational acceleration; $\overline{\theta}$ is resolved mean potential temperature; θ_0 is reference temperature; Ω_3 is Earth's rotation vector defined as $\Omega_3 = \omega[0, \cos\phi, \sin\phi]$, where ω is Earth's angular velocity and ϕ is the geographic latitude of the turbine site. The subgrid-scale stress tensor τ_{ij}^D is modeled using the Smagorinsky closure:

$$\tau_{ij}^D = -2\upsilon^{SGS}\overline{S}_{ij} \tag{3}$$

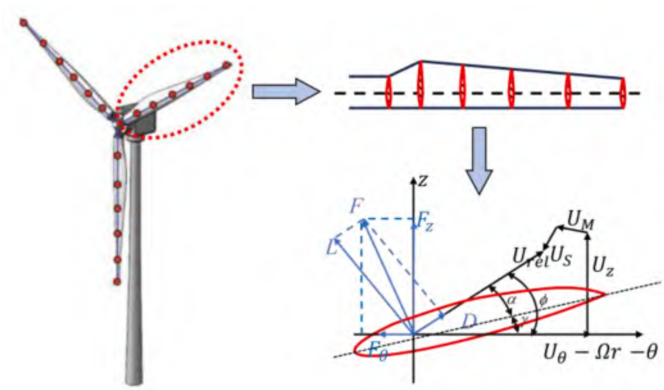

Fig. 1. Illustration of the actuator line method.

$$\nu^{SGS} = (C_s\Delta)^2\left(2\overline{S}_{ij}\overline{S}_{ij}\right)^{\frac{1}{2}} \tag{4}$$

with model constant $C_s = 0.13$, and the resolved strain rate tensor $\overline{S}_{ij}$ defined as:

$$\overline{S}_{ij} = \frac{1}{2}\left(\frac{\partial \overline{u}_i}{\partial x_j} + \frac{\partial \overline{u}_j}{\partial x_i}\right) \tag{5}$$

2.2.2. Modeling of rotating blades

Aerodynamic forces of the wind turbine blades are modeled using the actuator line method (ALM) developed by Sørensen and Shen (2002). This approach abstracts each turbine blade into discrete airfoil elements distributed along the spanwise direction (root to tip). For each element, blade element theory calculates aerodynamic forces based on the local relative wind velocity and angle of attack. The resulting force distribution is then projected onto the fluid domain as volumetric source terms in the momentum equations. This force projection employs a Gaussian smoothing kernel to distribute forces over adjacent grid cells, preventing numerical singularities while maintaining physical fidelity. An illustration of the ALM is provided in Fig. 1.

Compared to fully resolved blade simulations, ALM offers significant computational advantages while preserving essential wake dynamics: it eliminates boundary layer resolution requirements near blade surfaces while accurately capturing trailed vorticity effects through direct solution of Navier-Stokes equations. This balance of efficiency and accuracy makes ALM particularly suitable for far-wake investigations and has successfully applied to a wide range of wind turbine related researches (Troldborg, 2009), (Stevens et al., 2018), (Houtin-Mongrolle et al., 2020).

2.2.3. Simulation of wind turbine wake flow under atmospheric boundary layer (ABL)

To establish realistic inflow conditions for wind turbine wake simulation, this study implements a two-stage computational strategy (Lee et al., 2012) designed to generate a fully developed neutral atmospheric boundary layer (ABL), as shown in Fig. 2. The approach begins with a precursor large-eddy simulation (LES) that develops quasi-equilibrium turbulence statistics before introducing the wind turbine into the established flow field.

The computational domain is configured as a rectangular region spanning 24 rotor diameters (D = 126 m) in the streamwise direction (x-axis), 8D in the cross-flow direction (y-axis), and 8D in the vertical direction (z-axis), with the inflow aligned with the positive x-direction. Boundary conditions are carefully prescribed to maintain physical consistency: cyclic conditions are applied to the streamwise and spanwise boundaries to ensure periodicity, while the upper boundary employs a slip condition. The lower boundary utilizes the Moeng shear-stress model (Moeng, 1984) to accurately represent surface shear stress dynamics, critical for ABL development.

During the precursor simulation phase, a uniform grid resolution of 10 m in all directions facilitates efficient development of turbulence structures over an 18,300-s simulation period. The initial 18,000 s

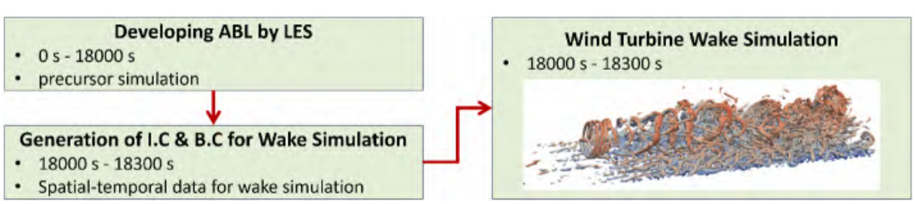

Fig. 2. Simulation procedure.

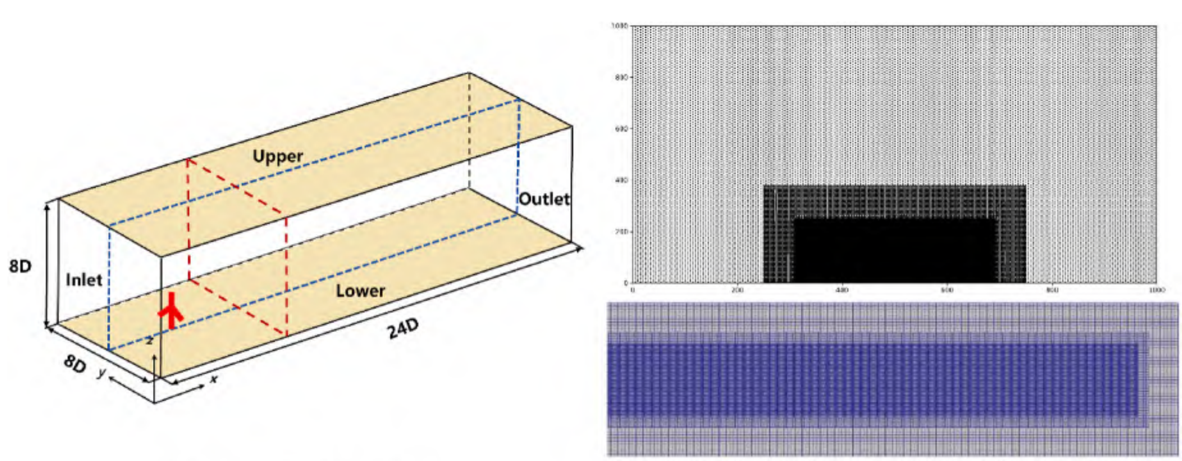

(a) computational domain

(b) computational cells on the indicated slice in (a): upper - red slice; lower - blue slice.

Fig. 3. Illustration of the computational domain and computational cells.

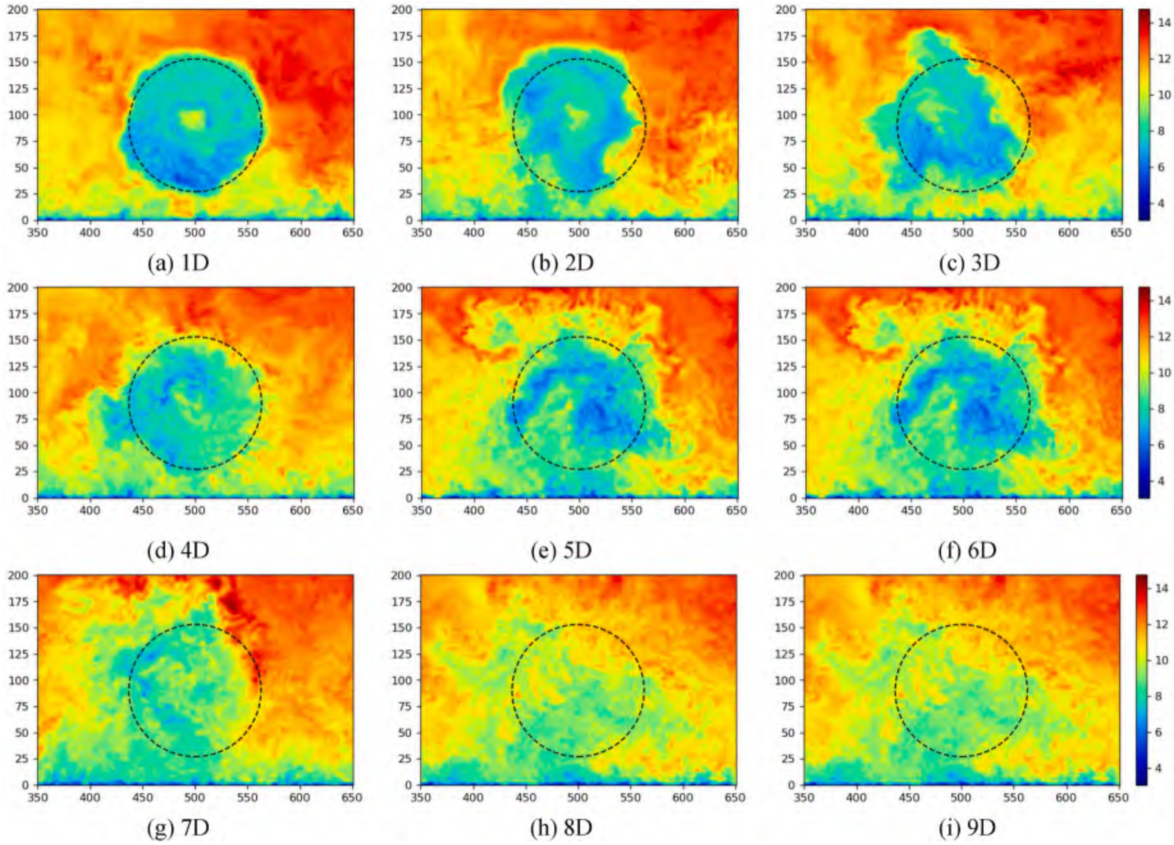

Fig. 4. CFD results.

establish statistically stationary turbulence, with the final 300 s providing the validated inflow conditions for subsequent turbine simulations. Temporal resolution is maintained at $\Delta t = 0.2$ s to adequately resolve turbulent eddies while ensuring computational feasibility. For the turbine-wake simulation phase, a mesh refinement is firstly applied to the computational domain to resolve critical flow features. Two refinement zones target the rotor area and wake development region: an inner region extending 2D vertically with 5 m resolution, surrounded by a secondary zone extending to 3D height with refined 2.5 m resolution. This multi-level refinement strategy ensures adequate resolution of blade-induced vortices while maintaining smooth grid transitions to minimize numerical instabilities. The optimized mesh comprises approximately 12 million computational cells. Wind turbine simulations are conducted over 300 physical seconds with a refined time step of 0.02 s to capture complicated multiscale wind turbine wake characteristics. An illustration of the computational domain and computational mesh used in the current study is shown in Fig. 3.

2.3. Simulation results

Fig. 4 presents a representative wake velocity profile at $t = 0$ s, demonstrating the complex turbulent structures captured by the LES-ALM approach. This instantaneous snapshot illustrates key wake characteristics including velocity deficit development, tip vortex evolution, and turbulent mixing layer formation under neutral ABL conditions.

Comprehensive validation studies of our CFD methodology - including grid convergence analysis, turbulence statistics verification, and comparison with experimental data - have been reported in our previous publications (Xu et al., 2022a), (Xu et al., 2022b), (Xu et al., 2024). These established studies confirm the accuracy of our simulation approach in capturing essential wake physics. As the present study focuses primarily on the novel hybrid physics-data framework for wake prediction, we will limit our CFD discussion to methodology description and representative results. The generated dataset contains 300 s (15,000 time steps) of high-resolution wake field data sampled at 14 downstream locations (1D-14D), providing the necessary inputs for neural network (NN) training and validation.

3. Modeling of wind turbine wake evolution by CNN-based encoder-decoder neural networks

3.1. Definition of neural network mapping relations

The purpose of the current study is to establish neural networks (NNs) that utilize sparse upstream measurements of wind turbine wake field as input to predict the downstream wake profiles, a framework we refer to as *wakeEvoNet*. Therefore, the mapping relation this paper aims to establish can be expressed as a function where the wake cross-section at a given downstream distance is predicted based on three consecutive upstream cross-sections:

$$section^{[n]D} = wakeEvoNet\left(section^{[n-3]D}, section^{[n-2]D}, section^{[n-1]D}\right) \tag{6}$$

in which.

- *wakeEvoNet* represents the mapping function established by neural networks (NNs);
- $section^{[n]D}$ denotes the wake cross-section at downstream distance n rotor-diameters (D);
- n indicates the target prediction location ($n \geq 4$)

This formulation establishes a sequential prediction paradigm where three consecutive wake profiles serve as input to forecast the subsequent downstream cross-section. This spatially decomposed framework enables the wake field to be progressively evolved from the measured near-

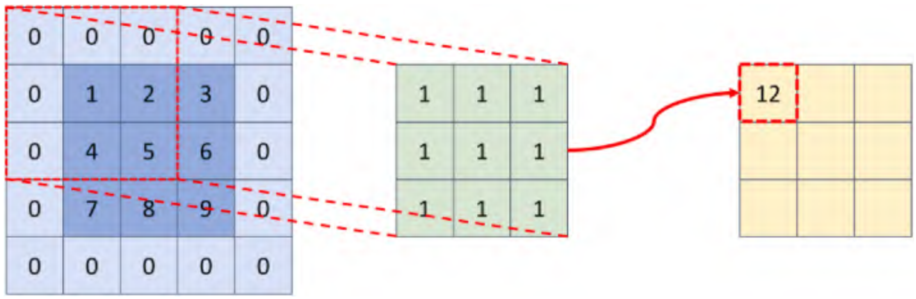

Fig. 5. Illustration of convolutional operation.

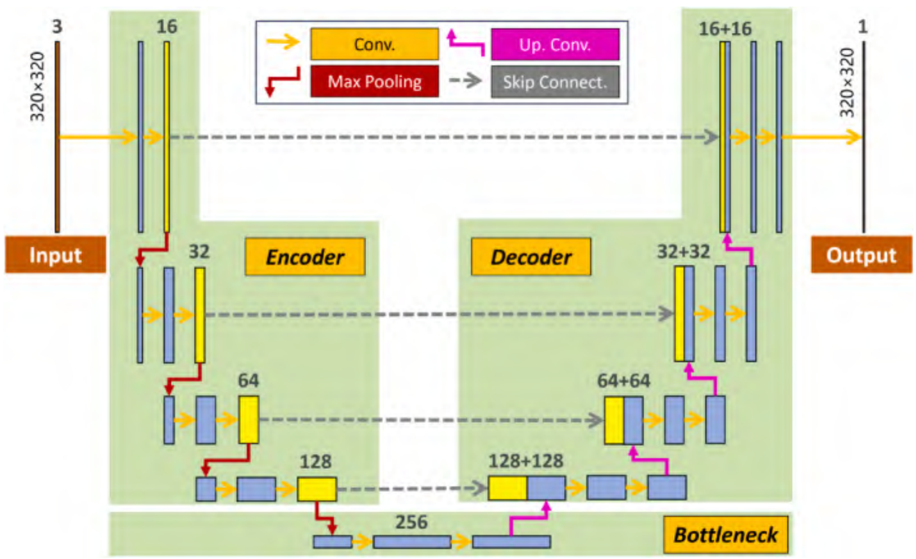

Fig. 6. Illustration of *wakeEvoNet*-1.

wake region (1D-3D) through the predicted far-wake region (4D-14D), creating an efficient rolling prediction scheme. It should be noted that the downstream coordinate origin is defined at the turbine rotor plane, and thus the 1D measurement plane corresponds exactly to $x/\ D = 1$ with no offset. For instance, feeding cross-sectional data from 7D, 8D, and 9D enables the prediction of the wake at 10D; subsequently, using sections from 8D, 9D, and the newly predicted 10D allows the model to forecast the wake at 11D, thereby autonomously generating a complete downstream wake field from limited upstream measurements. This approach effectively balances the need for physical accuracy in the complex near-wake region with computational efficiency for far-wake evolution.

3.2. *wakeEvoNet-1: A U-Net benchmark*

In this work, we employ the well-known U-Net (Ronneberger et al., 2015) architecture as our benchmark model, designated as *wake-EvoNet*-1, to establish a foundational performance baseline for wake evolution prediction. This convolutional neural network architecture is particularly suited for our task due to two fundamental characteristics that align well with the requirements of spatial flow field reconstruction. First, it utilizes convolutional operations for hierarchical feature extraction, enabling the model to capture multi-scale wake characteristics from the input cross-sectional data. Second, its symmetric encoder-decoder structure with skip connections facilitates both effective feature abstraction and precise spatial reconstruction, which is crucial for maintaining the physical coherence of the predicted wake fields. The encoder pathway progressively reduces spatial dimensions while increasing feature depth, effectively capturing contextual information about the wake structure, while the decoder pathway gradually recovers spatial resolution to generate high-fidelity predictions. This section will elaborate on these architectural components, beginning with the fundamental convolutional operations for feature extraction, followed by a detailed examination of the U-Net's encoder-decoder mechanism and its specific adaptation for wind turbine wake prediction tasks.

3.2.1. *The convolutional operation for feature-extraction*

Convolutional Neural Networks (CNNs) (LeCun and Bengio, 1998) represent a transformative advancement in deep learning, offering significantly accelerated training speeds and superior feature extraction capabilities compared to fully-connected neural networks. As fundamental building blocks for spatial data processing, CNNs have demonstrated exceptional performance across diverse domains including computer vision (Lecun et al., 2015), object identification (Ren et al., 2017), and flow field reconstruction (Brunton et al., 2020).

Specifically, for wind turbine wake tasks, CNN has three critical benefits for wake evolution modeling: (1) parameter efficiency: weight sharing dramatically reduces parameters versus fully-connected networks; (2) spatial Hierarchy: progressive abstraction captures wake diffusion patterns; (3) translation invariance: consistent feature detection regardless of wake position. These characteristics establish CNNs as the foundational architecture for our wake evolution framework, enabling efficient extraction of complicated wind turbine wake features from high-dimensional flow field data.

A standard CNN architecture processes input tensors $X \in \mathscr{R}^{H\times W\times C}$, where H, W, and C represent feature map height, width, and channel depth respectively. The convolutional operation extracts hierarchical spatial features through learnable kernels that traverse input feature maps via sliding-window operations. This process is mathematically defined as:

$$I'_{i,j} = \sigma\left(\sum_{m=-1}^{1}\sum_{n=-1}^{1}\left(w_{m,n} \times I_{i+m,j+n}\right) + b\right) \tag{7}$$

where $w_{m,n}$ represents kernel weights, b is the bias term, σ is the non-linear activation function. An illustration of the convolutional operation is presented in Fig. 5.

The spatial dimensionality evolution through convolutional layers follows:

$$H_{out} = \frac{H_{in} - KS + 2P}{S} + 1 \tag{8}$$

where K is kernel size, P is padding, and S is stride size.

3.2.2. The U-Net architecture

The *wakeEvoNet*-1 architecture employs the U-Net convolutional network as its foundational framework, originally developed for biomedical image segmentation (Ronneberger et al., 2015) but adapted here for high-resolution wake field prediction. This encoder-decoder structure features symmetric contracting and expanding pathways that enable precise spatial feature extraction and reconstruction essential for capturing complex wake dynamics. Three core components define its operational mechanism, i.e. the hierarchical feature abstraction (encoder) and a context-preserving decoder with skip-connections (more details of this architecture please refer to (Ronneberger et al., 2015)).

It should be mentioned here that compared to standard implementations, our adaptation incorporates a base channel of 16 instead of 64 in the original U-Net to conserve computational resources. The final output layer utilizes 1×1 convolution with linear activation to generate velocity field predictions at resolution matching input sections. This U-Net implementation achieves a parameter-efficient architecture (2 million parameters) while maintaining 320×320 spatial resolution throughout processing. As our benchmark model, it establishes baseline performance against which attention-enhanced variants are evaluated in Section 4. This refined implementation provides the baseline for our hybrid framework, balancing spatial fidelity with computational efficiency to establish the fundamental wake evolution capability before attention mechanism enhancements. An illustration of *wakeEvoNet*-1 is shown in Fig. 6.

3.3. Light-weight attention mechanisms

Attention mechanisms in deep learning can be broadly categorized into self-attention mechanisms and lightweight attention variants. While full self-attention mechanisms offer powerful global context modeling capabilities, they fall outside our consideration due to their prohibitive computational complexity and substantial parameter requirements, which are ill-suited for our application where available data volume is limited. Consequently, in the current work, we focus exclusively on lightweight attention mechanisms, which provide computationally efficient alternatives for feature refinement while maintaining manageable model complexity. These mechanisms enable selective emphasis on spatially significant regions within the flow field without introducing excessive computational overhead, making them particularly suitable for wind turbine wake prediction tasks where capturing critical flow structures is essential. The subsequent sections will detail our implementation of channel attention (CA), conventional spatial attention (SA), and our novel physics-guided Turbine-wake Attention (TA) mechanism, collectively designed to enhance feature representation within our encoder-decoder architecture while preserving computational feasibility.

3.3.1. The channel attention: CA

Let F ($F \in \mathscr{R}^{C\times H\times W}$) be the input feature map, in which, C represents the number of channels, H and W is the height and width of each channel, respectively, then, the operation of the CA can be mathematically written as:

$$CA = \sigma(FC(Avg\_P(\boldsymbol{F}))) + (FC(Max\_P(\boldsymbol{F}))) \tag{9}$$

where FC is a shared multi-layer perceptron (MLP) of which parameters can be adjusted in the training process, and,

$$Avg\_P(\boldsymbol{F}) = \frac{1}{H\times W}\sum_{i=0}^{H}\sum_{j=0}^{W}\boldsymbol{F}(i,j) \tag{10}$$

$$Max\_P(\boldsymbol{F}) = \max_{(i,j)}\boldsymbol{F}(i,j) \tag{11}$$

The final dimension of CA in Eq. (9) is: $C\times1\times1$. Then, CA is applied to the original feature map $\boldsymbol{F}$ as described by the following equation:

$$\boldsymbol{F}' = CA\bigotimes\boldsymbol{F} \tag{12}$$

where $\boldsymbol{F}'$ is the CA-refined feature map, and $\bigotimes$ represents element-wise multiplication.

3.3.2. The original spatial attention mechanism: SA

Let F ($F \in \mathscr{R}^{C\times H\times W}$) be the input feature map, in which, C represents the number of channels, H and W is the height and width of each channel, respectively, then, the operation of the spatial attention (SA) can be mathematically written as:

$$SA = \sigma\left(\mathrm{conv}^{7\times7}\left(\mathrm{concat}\left[\mathrm{Avg\_CP}(\boldsymbol{F});\mathrm{Max\_CP}(\boldsymbol{F})\right]\right)\right) \tag{13}$$

where Avg_CP($\boldsymbol{F}'$) and Max_CP($\boldsymbol{F}'$) represents the channel-wise average and max pooling operation, defined as:

$$Avg\_CP(\boldsymbol{F}) = \frac{1}{C}\sum_{c=1}^{C}\boldsymbol{F}(:,:) \tag{14}$$

$$Max\_CP(\boldsymbol{F}) = \max_{c}\boldsymbol{F}(:,:) \tag{15}$$

in which $\boldsymbol{F}(:,:)$ represents the pooling operation is performed for each channel. Therefore, the final dimension of SA is: $1\times H\times W$. Then, SA is applied to $\boldsymbol{F}$ to obtain the final $\boldsymbol{F}'$ as described by the following equation:

$$\boldsymbol{F}' = SA\bigotimes\boldsymbol{F} \tag{16}$$

3.3.3. A physics-guided light-weight spatial attention: TA (Turbine-wake attention)

The above-mentioned spatial attention utilizes max and average pooling operations to integrate the attention mechanism for each channel. However, these two operations may be too elementary for wind turbine wake flows, this approach prioritize cross-channel feature importance rather than local flow physics. Wind turbine wake flows are turbulent and being famous for their multiscale nature, therefore, a refinement of spatial attention to efficiently capture complicated flow features is required for the current task. As an attempt to address this limitation, in the current work, we propose a potential alternative to the traditional SA mechanism, i.e. the Turbine-wake Attention (TA) mechanism - a physics-guided lightweight, flow-adaptive spatial attention module specifically designed for wind turbine wake characteristics that dynamically weights complicated flow characteristics based on local velocity features. Similarly, let F ($F \in \mathscr{R}^{C\times H\times W}$) be the input feature map, in which, C represents the number of channels, H and W is the height and width of each channel, respectively, the mathematical formulation of the TA operation can be expressed as follows:

1. Feature conditioning:

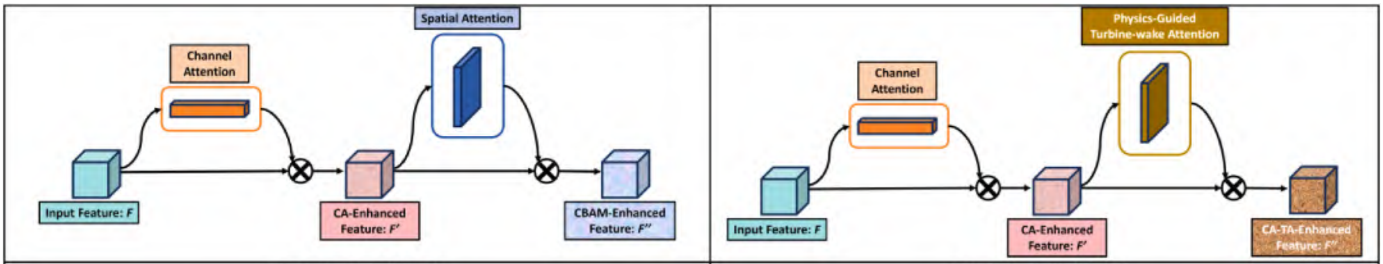

(a) CBAM block. (b) CA-TA block.

Fig. 7. Integration of channel and spatial mechanisms.

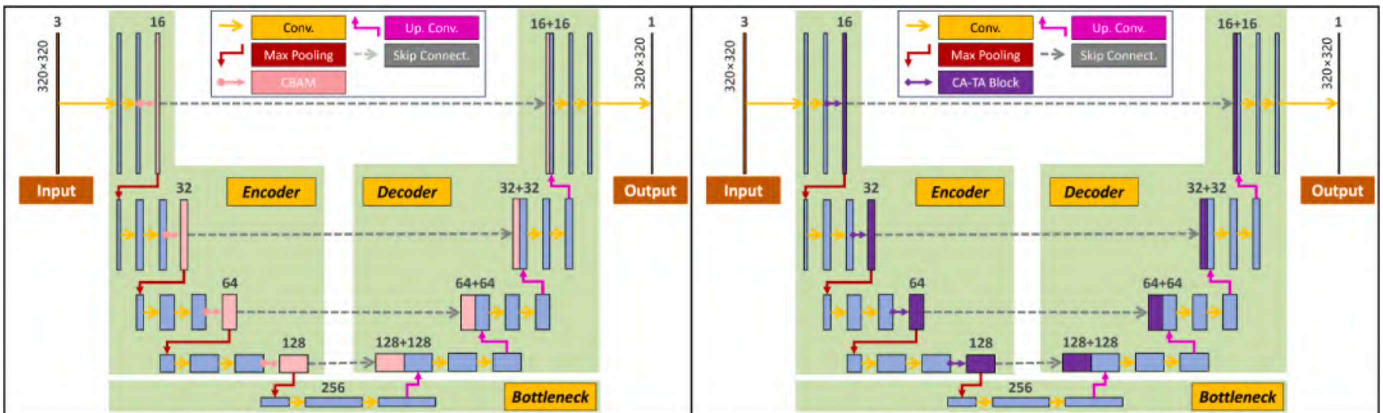

(a) *wakeEvoNet*-2: CBAM-UNet (b) *wakeEvoNet*-3: CA-TA-UNet

Fig. 8. Illustration of attention-enhanced U-Nets.

$$intensity(\boldsymbol{F}) = \text{sigmoid}\left(\text{conv}^{5\times5}\left(\text{Relu}\left(\text{conv}^{3\times3}(\boldsymbol{F})\right)\right)\right) \tag{17}$$

2. Adaptive flow feature scaling:

$$scale = Parameter \times intensity(\boldsymbol{F}) \tag{18}$$

where *Parameter* is trainable, and it can be realized by using nn. Parameter(.) function in pyTorch.

3. Attention integration:

$$TA = 1.0 + scale \tag{19}$$

$$\boldsymbol{F}' = TA \otimes \boldsymbol{F} \tag{20}$$

This formulation enables velocity-adaptive feature amplification, where regions exhibiting stronger flow-velocity gradients receive enhanced weighting during wake evolution prediction. Notably, the computed $intensity(\boldsymbol{F})$ - containing trainable parameters through a sigmoid activation - remains constrained to the interval [0, 1]. The subsequent scaling multiplication with *Parameter* thus expands the effective range of *TA* values, deliberately emphasizing spatially influential positions through dynamic calibration. This design provides essential flexibility for modeling wind turbine wake flows under ABL conditions, where multi-scale flow regimes exist due to high ambient turbulence.

Crucially, the velocity-adaptive weighting mechanism of TA is intrinsically aligned with the fundamental physical characteristics of wind turbine wakes. The attention weights generated by TA are dynamically distributed to prioritize three physically critical regions: (1) the central wake zone with pronounced velocity deficit, where the flow speed is substantially reduced by the turbine rotor; (2) the annular shear layers surrounding the wake core, where sharp velocity gradients dominate turbulent mixing and wake diffusion; and (3) the radial boundaries corresponding to wake expansion along the downstream direction. By amplifying feature responses in these regions that govern wake evolution dynamics, the TA module discards generic spatial pooling operations and establishes a direct link between attention weighting and underlying flow physics. This physics-based feature weighting strategy serves as the core rationale for describing the proposed module as “physics-guided”, ensuring the network concentrates on physically meaningful flow structures rather than learning non-physical patterns.

To summary, its design leverages the following key principles.

- Local turbulence representation: Turbulence manifests as localized distortions in images, such as blurring, shimmering, or warping. The module uses a small convolutional network with a 3×3 kernel to capture these local spatial patterns. The first convolutional layer reduces the channel dimension, focusing the network on salient local features, while the subsequent 1×1 convolution generates a single-channel intensity map. This design mimics the physical behavior of turbulence, which often exhibits localized effects
- Intensity-based adaptive weighting: Unlike traditional spatial attention, which often suppresses less important regions, this module uses a baseline weight of 1.0 and adds a scaled intensity term: weights $= 1.0 +$ scale $\times$ intensity. This ensures that regions with high turbulence intensity are enhanced rather than suppressed, as these areas typically correspond to significant degradation that requires stronger feature refinement. The learnable scale parameter allows the model to adapt the enhancement magnitude dynamically during training

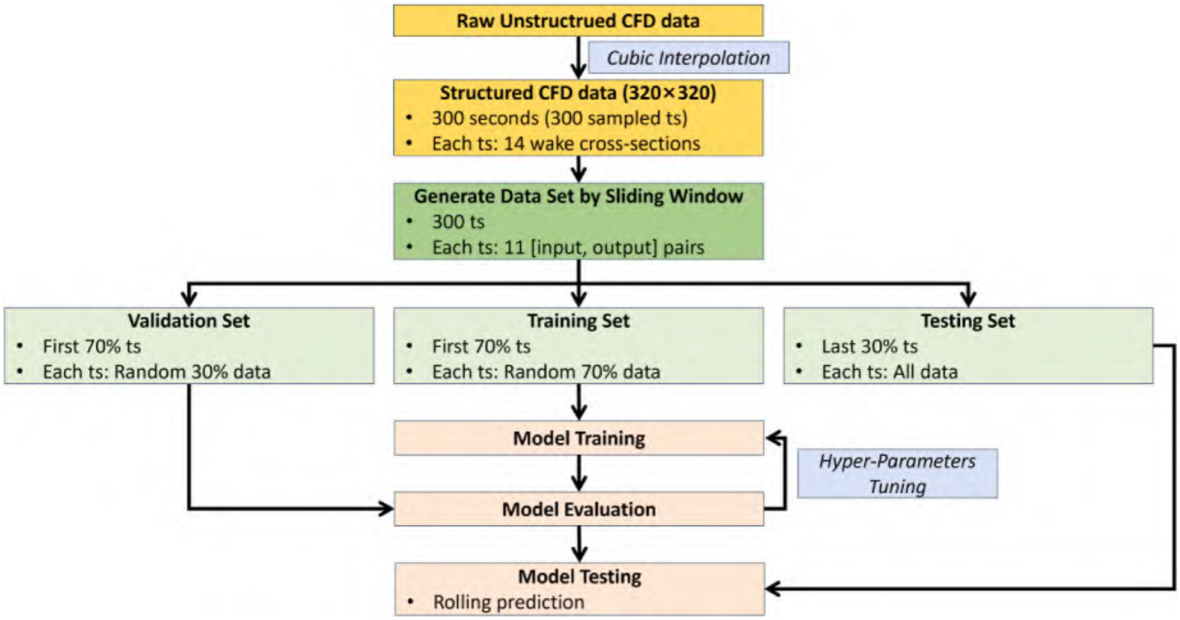

Fig. 9. Dataset preparation.

3.4. *wakeEvoNet*-2 & *wakeEvoNet*-3: improved U-Nets by light-weight attentions for wind turbine wake prediction

3.4.1. Integration of channel and spatial attention mechanisms

This subsection focuses on the integration of channel and spatial attention mechanisms to enhance feature representation in neural networks. Building upon the established channel attention, spatial attention (SA), and turbine-wake attention (TA) components described previously, we combine these mechanisms into cohesive integrated blocks that operate synergistically within the network architecture. Fig. 7 provides a visual comparison of two such integrated attention blocks, where subfigure (a) illustrates the standard Convolutional Block Attention Module (CBAM) block, with comprehensive details available in Reference (Woo et al., 2018). Upon comparison with the CBAM block, it becomes apparent that the two integrated blocks share identical structures and operational principles, with the only distinction lying in the specific methodology employed for incorporating the SA and TA components, allowing for a controlled-variable comparison in the subsequent analysis.

3.4.2. Attention enhanced U-Nets

Fig. 8 presents the architecture of attention-enhanced U-Nets, which are developed by integrating specialized attention blocks into the baseline *wakeEvoNet*-1 model to improve feature representation for wake prediction. Specifically, the Convolutional Block Attention Module (CBAM) is incorporated to create *wakeEvoNet*-2, while the custom Channel Attention-Turbine-wake Attention (CA-TA) block is integrated to form *wakeEvoNet*-3, with both variants designed to enhance the model's ability to focus on critical flow regions. In Fig. 8, subfigure (a) illustrates *wakeEvoNet*-2 and subfigure (b) depicts *wakeEvoNet*-3, demonstrating that the two models maintain identical structural frameworks except for the spatial attention mechanism; *wakeEvoNet*-2 utilizes the standard spatial attention from CBAM, whereas *wakeEvoNet*-3 employs the physics-guided Turbine-wake Attention (TA) proposed in this study, enabling a direct evaluation of the TA mechanism's impact on performance.

4. Results and discussion

4.1. Model training

4.1.1. Preparation of datasets

The CFD simulation data is first preprocessed to prepare the datasets for NN training. The data obtained from CFD simulations is stored in an unstructured-grid sense (Fig. 3(b)), therefore, conversion from unstructured data to structured format was performed using cubic interpolation to meet the input requirements of CNNs. Subsequently, velocity profiles spanning 300 s (sampled as 300 timesteps) were systematically re-formatted across 14 downstream monitoring locations (1D to 14D). A sliding-window methodology is used to generate the {input, output} pairs which were defined in Eq. (6). For each timestep, 11 sequential data samples were constructed in the form $\{\text{Input}: (\mathit{section}^{[n-3]D}, \mathit{section}^{[n-2]D}, \mathit{section}^{[n-1]D}), \text{Output}: (\mathit{section}^{[n]D})\}$, where the positional index n ranged from 4 to 11. The stacking of these samples yields a dataset containing 3300 training samples.

This comprehensive dataset is then split to ensure rigorous model training and evaluation. The temporal domain was segmented into two datasets: simulations from 1 to 210 s (70% duration) formed the training and validation datasets, while the remaining 90 s (211–300 s, 30% duration) constituted a temporally independent test dataset. Further, within the initial 210-s period, 7 randomly selected sample pairs per timestep (1470 total samples) comprised the training dataset, with the other 4 pairs per timestep (840 samples) reserved for validation purposes. The test dataset incorporated all 11 sample pairs across the final 90 timesteps, in total 990 samples for the assessment of generalization capability of the trained NN models. The above description of dataset preparation can be illustrated by using Fig. 9.

4.1.2. Training specifications

Prior to model training, Min-Max normalization was applied to all input wake velocity cross-sections to standardize the data range and stabilize the CNN training process. Specifically, raw velocity values were linearly scaled to the fixed interval [0, 1] using the global minimum and maximum velocity values computed from the entire training dataset:

$$u_{\text{norm}} = \frac{u - u_{\min}}{u_{\max} - u_{\min}} \tag{21}$$

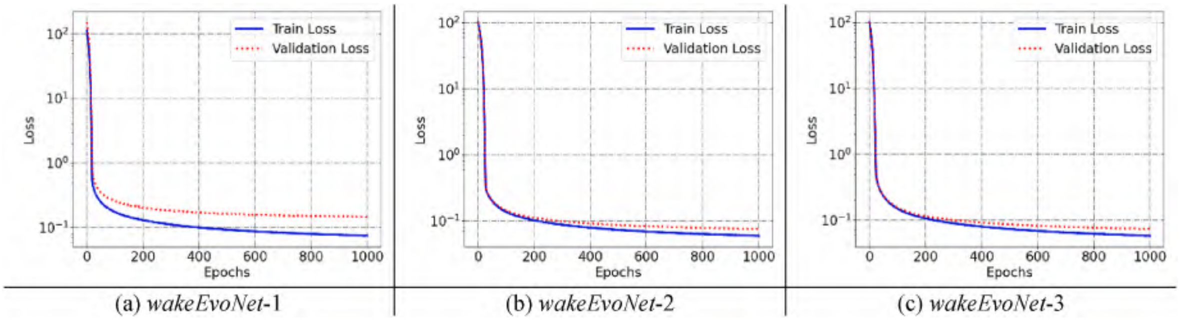

Fig. 10. Change of loss functions in the training process.

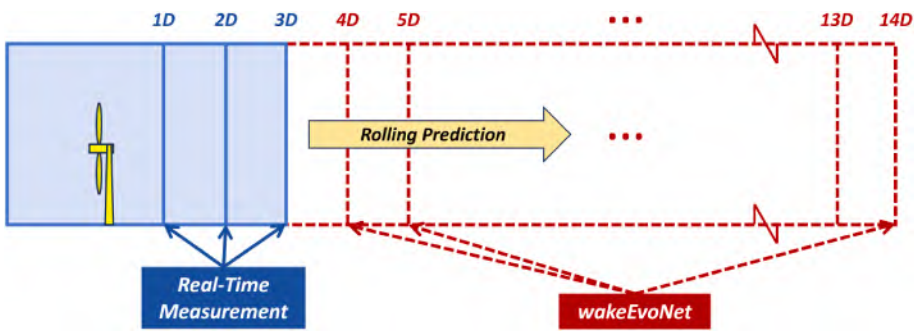

Fig. 11. Illustration of rolling prediction.

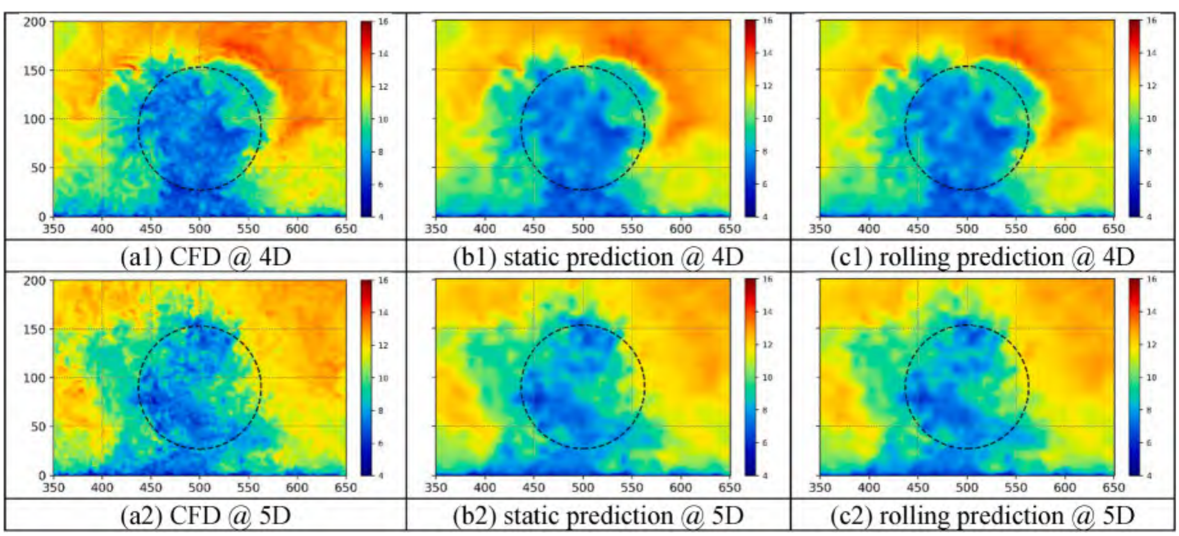

Fig. 12. Comparison of rolling prediction and static prediction.

where u denotes the raw velocity magnitude, $u_{\min}$ and $u_{\max}$ represent the global minimum and maximum velocity values across all training samples, respectively. This normalization unifies the numerical scale of input flow fields and accelerates the convergence of gradient-based optimization.

The model optimization process employed the root mean square error (ERMS) as the loss function, which is defined by Eq. (22). This metric quantifies the discrepancy between predicted and ground-truth velocity fields (CFD results in the current work) by computing the square root of the average squared differences across all spatial grid points.

$$E_{RMS} = \sqrt{\frac{1}{m}\sum_{i=1}^{m}\left(y_i - y_i^{pred}\right)^2} \tag{22}$$

All neural network architectures utilized the Rectified Linear Unit (*ReLU*) activation function specified in Eq. (23) for hidden layers, which introduces non-linearity while maintaining computational efficiency through its piecewise linear operation. This activation choice facilitates gradient flow during backpropagation and mitigates vanishing gradient issues common in deep architectures. The final output layer employed linear activation to enable continuous velocity predictions without range constraints.

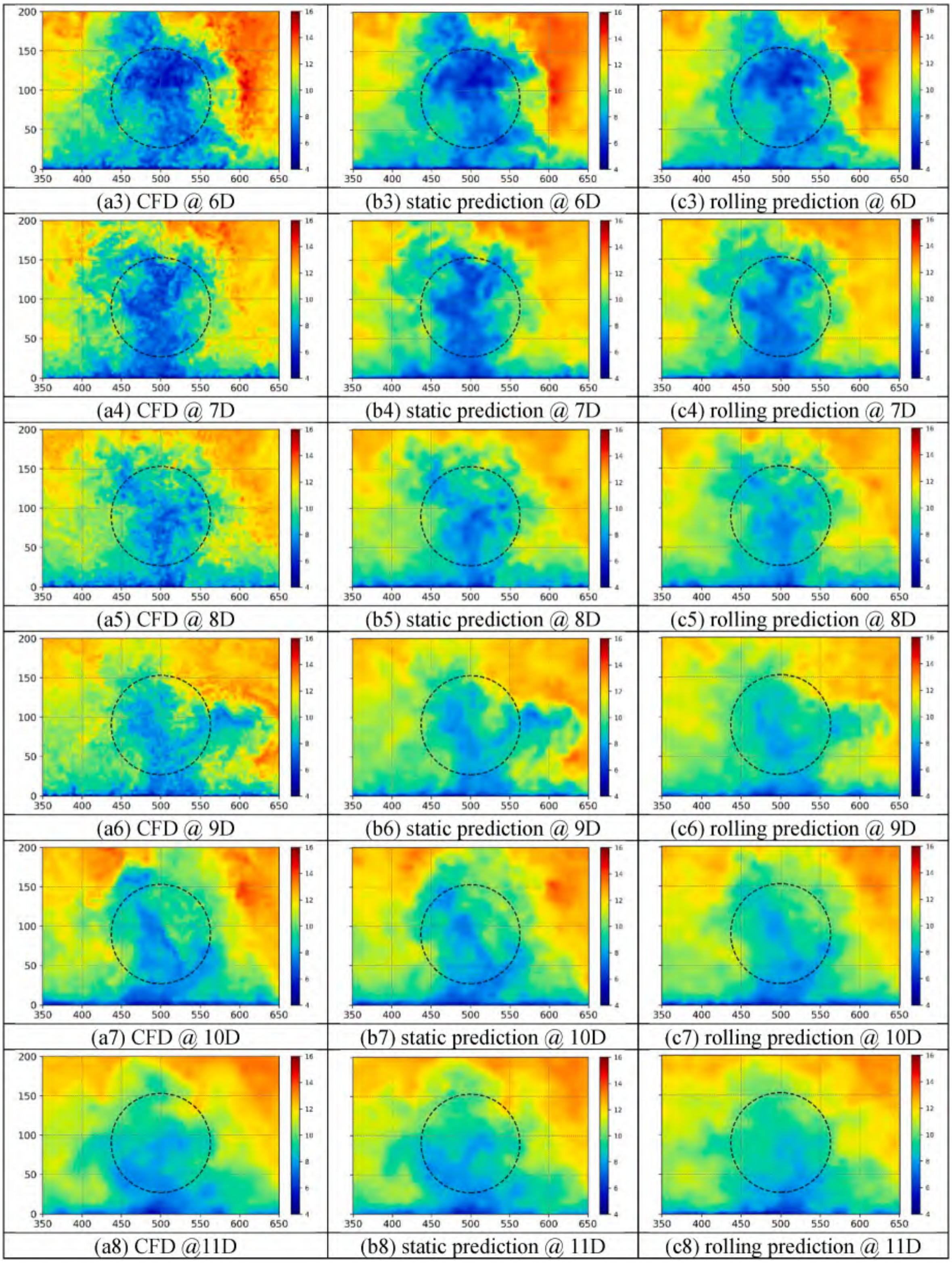

Fig. 12. (*continued*).

$$ReLU(x) = max(0, x) \tag{23}$$

Prior to model training, Min-Max normalization was applied to all input wake velocity cross-sections to standardize the data range and stabilize the CNN training process. Specifically, raw velocity values were linearly scaled to the fixed interval [0, 1] using the global minimum and maximum velocity values computed from the entire training dataset.

4.1.3. Training results

Model optimization was implemented using PyTorch's Adamax algorithm, a variant of the Adam optimizer that leverages the infinity norm for gradient normalization. This optimizer demonstrates superior convergence properties for problems with sparse gradients and noisy data characteristics inherent to turbulent wake fields. The training regimen incorporated validation-based early stopping with a patience

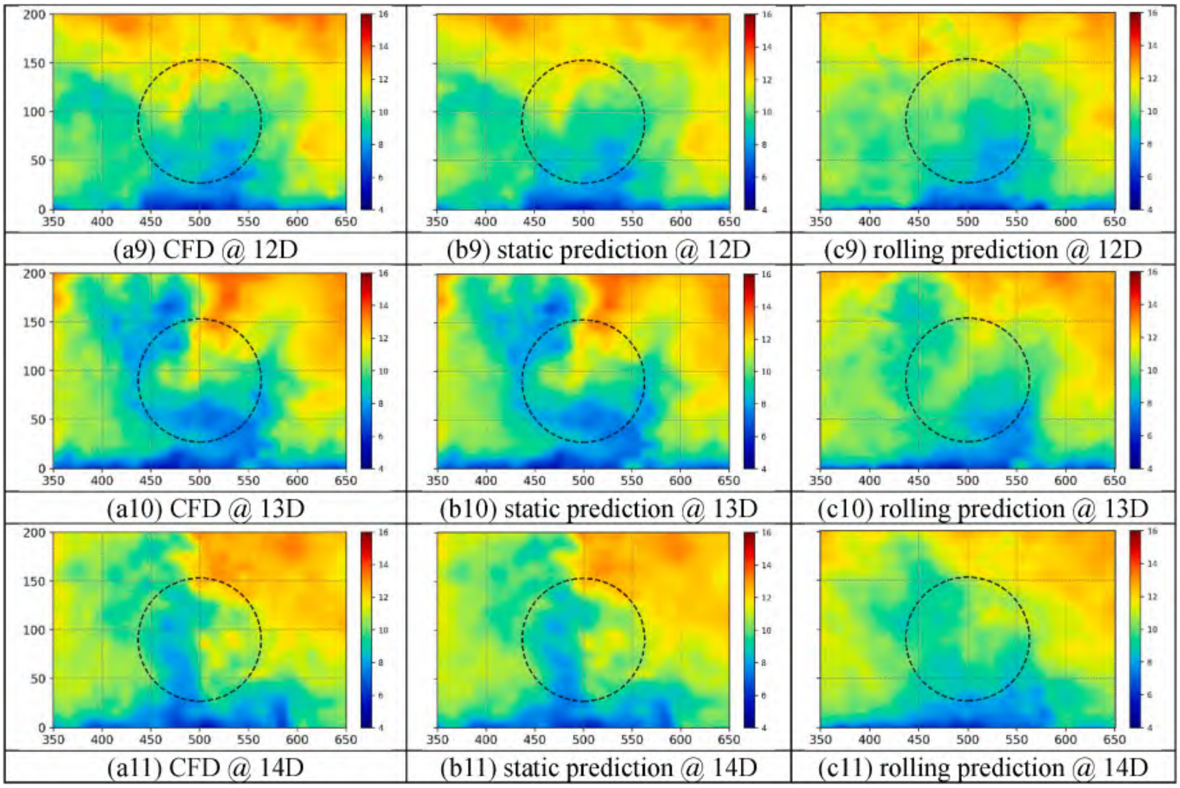

Fig. 12. (*continued*).

threshold of 25 epochs to prevent overfitting while ensuring parameter convergence. The training progression for all *wakeEvoNet* variants is depicted in Fig. 10, which illustrates the decrease of both training and validation losses across 1000 epochs. This convergence behavior confirms effective learning without overfitting, as evidenced by the parallel reduction of training and validation curves. The eventual stabilization of losses below 0.1 indicates successful optimization of the NN mapping function as described by Eq. (6).

4.2. Model evaluation

This section presents a comprehensive evaluation of the three trained neural network models—*wakeEvoNet*-1, *wakeEvoNet*-2, and *wakeEvoNet*-3—to systematically assess their predictive capabilities for wind turbine wake evolution.

4.2.1. Clarification of sequence prediction schemes

Prior to conducting the evaluation, it is imperative to clarify the fundamental prediction methodology employed in this study. Based on our examination of existing literature on sequence prediction, we observe that many studies fail to adequately distinguish between different prediction schemes, potentially leading to optimistically biased results that may not reflect practical operational scenarios. In general, two different prediction strategies exist in the prediction of sequential data, i.e. the static prediction and rolling prediction. In the static prediction, ground truth data is continuously fed as input to predict the later data of a sequence. For instance, in weather prediction tasks, one can feed updated real data into weather prediction models, say the latest 24 h, to predict the temperature in the next hour. And then after 1 h later, the newest 1-h measured data can be feed into the model. However, in our task, this static prediction method should not be applied because our goal is to build a hybrid physics-data framework in which the costly On-site monitoring should be confined within the near-field (1D - 3D) of the wind turbine wake. Therefore, in the current study, the approach of rolling prediction - a methodology where model outputs at preceding downstream sections serve as inputs for subsequent predictions - should be applied, although the readers may immediately realize that the accuracy of the results obtained by rolling prediction is lower than static prediction due to the accumulation of errors.

An illustration of the rolling prediction is shown in Fig. 11. As can be observed in the figure, high-fidelity while sparse on-site measurement is confined within the blue region. This methodological distinction is visually substantiated in Fig. 12, where qualitive comparisons between rolling and static prediction approaches reveal a systematic accuracy degradation in rolling predictions due to prediction error accumulation.

While static prediction demonstrates superior accuracy by circumventing error accumulation, it represents an unrealistic operational scenario for our hybrid data-physics framework. The rolling prediction implementation, despite its inherent accuracy challenges, provides a faithful validation of the framework's practical utility in spatially decomposed predictions where only near-wake measured data (1D - 3D) is available to initiate far-wake evolution. In the remaining of this subsection, the performances of the three trained NN models are quantified in terms of (1) spatial accuracy, (2) temporal consistency, and (3) error distribution.

4.2.2. Spatial accuracy

The spatial accuracy of *wakeEvoNet* predictions was systematically evaluated through comprehensive quantitative and qualitative analyses across the entire testing dataset ($t = 211 - 300$ s). Fig. 13 presents a comparative visualization of instantaneous wake velocity fields at all NN-predicted downstream locations (4D-14D) for the *wakeEvoNet*-1, *wakeEvoNet*-2, and *wakeEvoNet*-3 against ground truth (CFD results). It should be noted that all subplots in Fig. 13 employ an identical colorbar scale. To enlarge each subfigure to the fullest extent and enhance visual clarity for editorial formatting, colorbars are exclusively displayed for ground truth cases and omitted from NN prediction results. This visual comparison reveals three fundamental insights regarding the models'

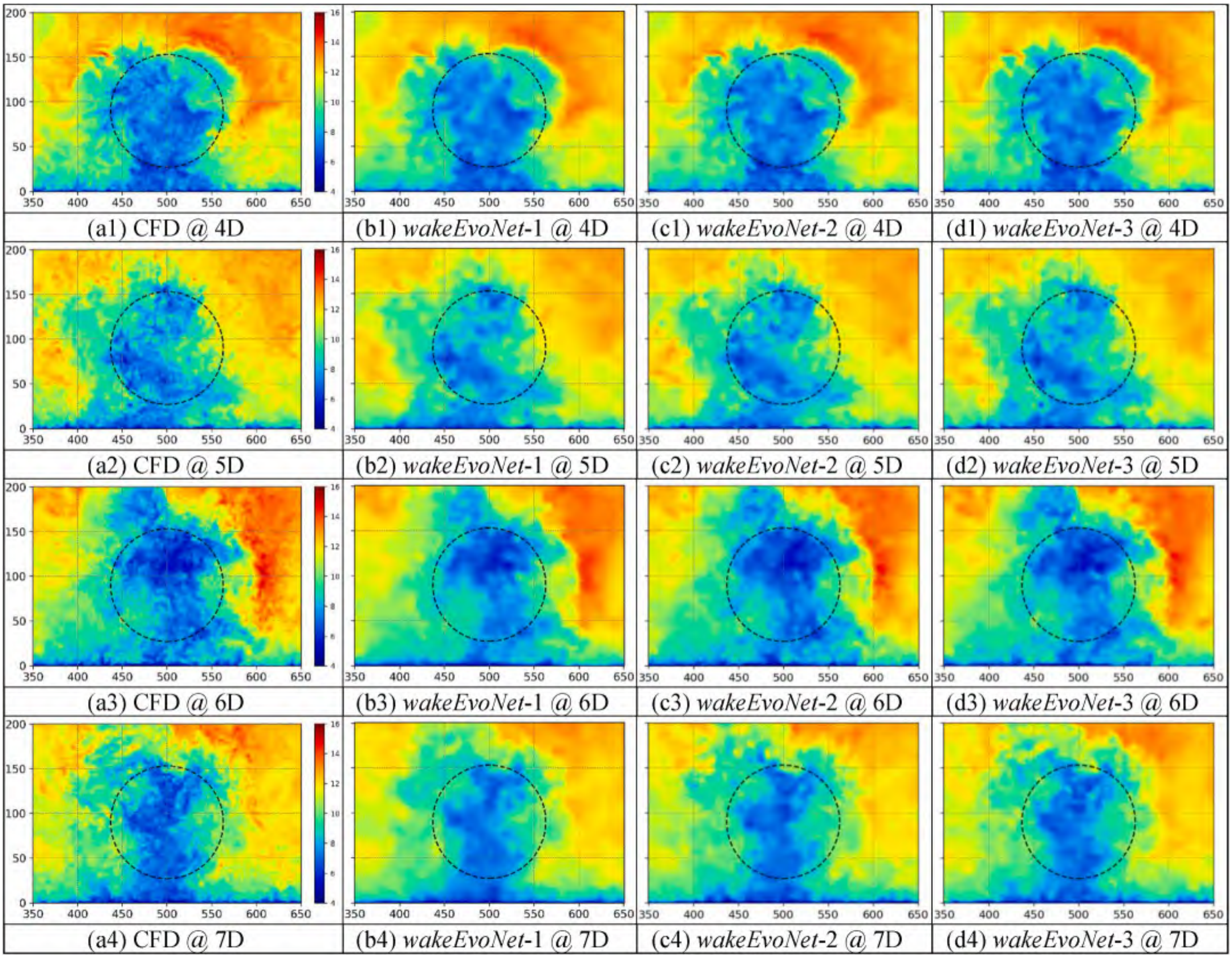

Fig. 13. Comparison of different models at different downstream locations.

capability to resolve wake dynamics: (1) All architectures successfully capture large-scale wake features including the velocity deficit core and primary shear layer evolution; (2) Resolution of small-scale turbulent structures progressively degrades with increasing downstream distance due to error accumulation in rolling prediction; (3) *wakeEvoNet*-3 demonstrates superior preservation of fine-scale flow features, particularly beyond the distance of 9D.

Quantitative validation employed two complementary metrics computed across all test samples: the spatially averaged root-mean-square error (E_{RMS}) and coefficient of determination (R^2). These metrics were calculated through ensemble averaging over the 990 test samples as defined in Eq. (24) and Eq. (26):

$$E_{RMS} = \frac{1}{TS}\sum_{j=1}^{TS} E_{RMS}^{j} \tag{24}$$

where TS is the total number of samples in the testing dataset, i.e. $TS = 990$ in the current study, and for the jth cross section, or sample, E_{RMS}^{j} is defined as:

$$E_{RMS}^{j} = \sqrt{\frac{1}{N}\sum_{i=1}^{N}\left(u_i - u_i^{pred}\right)^2} \tag{25}$$

where N is the total number of points in one cross-section, i.e. $N = 320 \times 320$ in the present study, u_i is the velocity obtained by CFD, i.e. the ground truth, and u_i^{pred} is the velocity predicted by the NN models.

R^2 is defined as:

$$R^2 = \frac{1}{TS}\sum_{j=1}^{TS}\left(R_j^2\right) \tag{26}$$

where, similarly, for the jth cross section, or sample, R_j^2 is defined as:

$$R_j^2 = 1 - \frac{\sum_{i=1}^{N}\left(u_i - u_i^{pred}\right)^2}{\sum_{i=1}^{N}\left(u_i - \overline{u_i}\right)^2} \tag{27}$$

It should be noted that the range of R^2-score is [0, 1], and a value closer to 1 indicates a higher goodness of fit for the model.

Table 1 presents the downstream evolution of these metrics (written as E_{RMS}/R^2 in Table 1) across all the three trained NN models. A visualization of the table is provided in Fig. 14. In Fig. 14, following observations can be obtained:

- *wakeEvoNet*-3 consistently outperformed both *wakeEvoNet*-1 and *wakeEvoNet*-2 across all the downstream distances, achieving

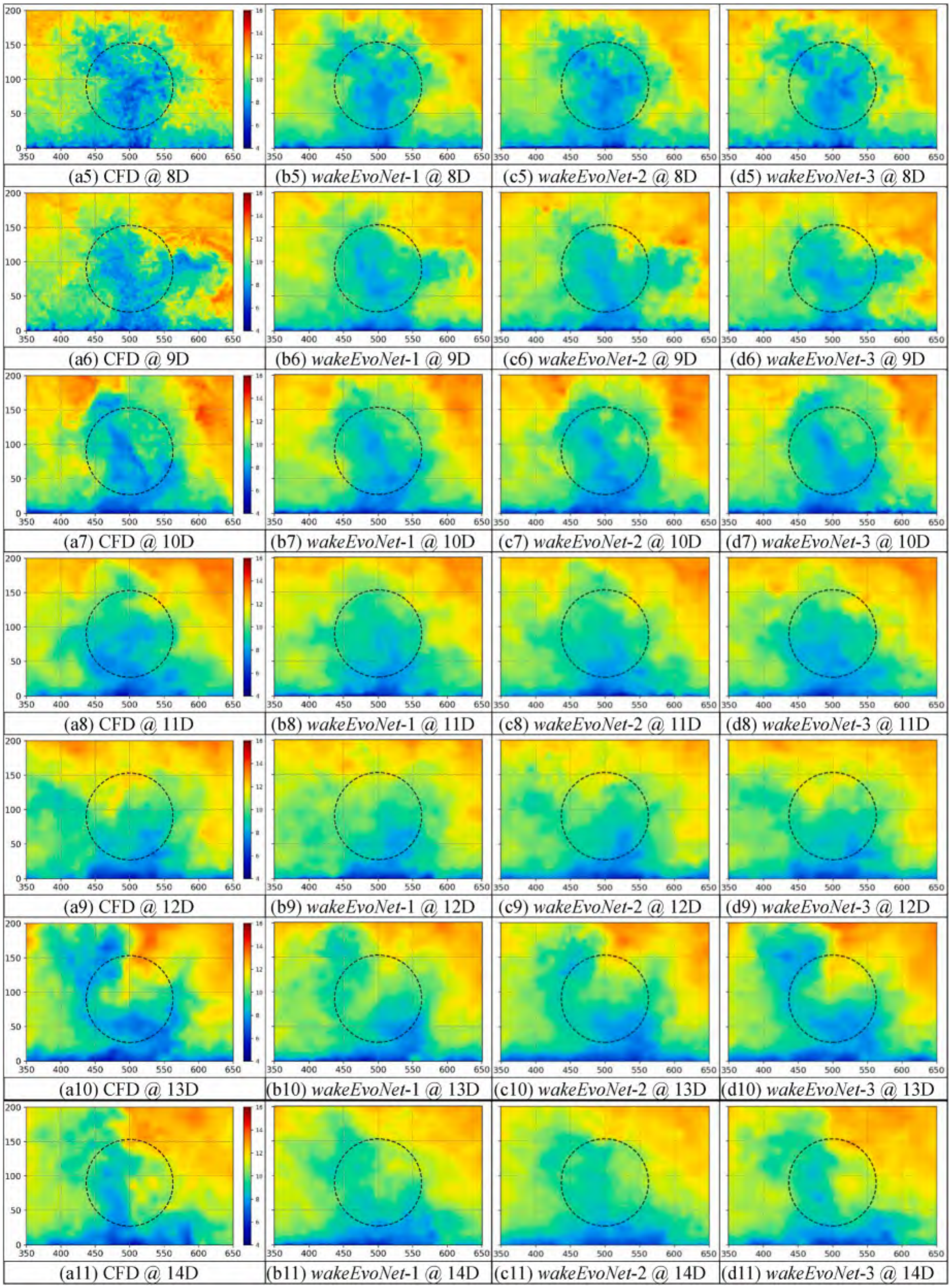

Fig. 13. (*continued*).

maximum R^2 superiority of 17.5% at 13D compared to *wakeEvoNet*-1. This performance advantage is particularly pronounced beyond 9D, demonstrating the TA mechanism's efficacy in preserving physical coherence during extended evolution. The CBAM-UNet (*wakeEvoNet*-2) shows intermediate performance, exceeding the baseline U-Net (*wakeEvoNet*-1) by 5-10% R^2 at mid-range distances (8D-12D) but failing to match *wakeEvoNet*-3's robustness in far-wake regions.

- All models exhibit characteristic accuracy decay with increasing downstream distance, consistent with error accumulation in rolling prediction. Mean R^2 decreases from approximately 0.98 at 4D to

Table 1
E_{RMS} and R^2-scores at different downstream locations obtained by different models.

	wakeEvoNet-1	*wakeEvoNet*-2	*wakeEvoNet*-3
4D	0.2995/0.9805	0.2480/0.9866	0.2712/0.9838
5D	0.3849/0.9573	0.3328/0.9681	0.2615/0.9831
6D	0.4716/0.9555	0.4226/0.9643	0.3079/0.9791
7D	0.5021/0.9289	0.5075/0.9274	0.3369/0.9474
8D	0.5072/0.9075	0.5045/0.9085	0.3226/0.9417
9D	0.5752/0.8746	0.5518/0.8846	0.4722/0.9051
10D	0.5515/0.9009	0.5001/0.9185	0.3687/0.9410
11D	0.4700/0.9174	0.4368/0.9286	0.4100/0.9330
12D	0.5602/0.8621	0.4615/0.9064	0.4537/0.9150
13D	0.8300/0.7584	0.6570/0.8486	0.4547/0.9335
14D	0.7077/0.7777	0.6452/0.8152	0.5364/0.8552

approximately 0.85 at 14D for *wakeEvoNet*-3, with more severe degradation observed in baseline models (*wakeEvoNet*-1: 0.98 to 0.78).

- Non-monotonic error progression is also observed. Contrary to expected monotonic decay, all models exhibit localized accuracy recovery at 10D ($R^{2}\approx 0.94$ for *wakeEvoNet*-3) following performance minima at 9D ($R^{2}\approx 0.90$). As to the authors understanding, this anomaly may suggest inherent flow physics governs prediction stability: the wake evolution operator demonstrates varying sensitivity to input conditions at different development stages. The recovery at 10D may indicates greater dependence on earlier inputs (7D-8D sections) than immediate predecessors, providing resilience against localized error spikes. Further work in the future to quantify the dependency, or correlation, of different wake cross-sections will be conducted.

4.2.3. Temporal consistency

This section evaluates the temporal robustness of *wakeEvoNet* predictions by examining performance stability across evolving wake conditions at fixed downstream locations. While spatial accuracy analysis in Section 4.2.2 quantified performance variations along the streamwise direction, temporal consistency assesses whether prediction quality degrades systematically as simulation time progresses – a critical validation for practical deployment where wake evolution models must maintain accuracy throughout extended operational periods.

Fig. 15 presents instantaneous wake predictions at 10D across five representative time instances ($t = 0$, 80, 160, 240, and 300 s). The figures reveal no visually discernible differences among the three trained NN models as time progresses. To rigorously evaluate temporal consistency across simulation time, we systematically quantify prediction accuracy metrics (E_{RMS} and R^2-scores) at each timestep for all downstream cross-sections spanning 4D to 14D. These time-resolved accuracy measurements are visualized in Fig. 16. Each subfigure corresponds to a specific downstream position (4D through 14D), enabling direct comparison of temporal patterns across the wake development region. Within each subfigure, solid lines represent the R^2-scores, while dashed lines indicate E_{RMS}. Additionally, blue backgrounds indicate the training dataset domain, whereas red backgrounds represent the test dataset, which remained unseen by the models during training.

The following observations emerge by scrutinizing Fig. 16.

- All models maintain stable performance throughout the 90-s test period, with *wakeEvoNet*-3 exhibiting minimal temporal variance of R^2 (denoted by σ hereafter). The absence of systematic degradation confirms the framework's robustness against temporal error accumulation - a critical advantage over recurrent neural network approaches that typically suffer from vanishing gradient problems during extended simulations. This stability stems from our spatial-decomposition strategy which resets error accumulation at each prediction step through renewed real-time monitored data of the near-wake region.
- *wakeEvoNet*-3 demonstrates significantly improved temporal consistency (10-50% lower variance) compared to *wakeEvoNet*-1 across all evaluated positions. This stability enhancement is particularly pronounced at 13D (*wakeEvoNet*-3 $\sigma = 0.0121$ vs. *wakeEvoNet*-1 $\sigma = 0.0568$). The TA mechanism's flow-adaptive feature weighting provides intrinsic robustness to temporal flow variations by dynamically adapting important flow features that dominate wake transport physics.

The above observations demonstrate that our hybrid physics-data framework maintains temporal stability without performance degradation throughout extended time periods. The spatial-decomposition approach fundamentally restricts, or confines, temporal error propagation by periodically re-initializing predictions with real-time measured data, while the turbine-wake attention (TA) mechanism proposed in the current study provides adaptive robustness to inflow variations. This hybrid approach represents a significant advancement over conventional data-driven methods, which typically exhibit degrading accuracy during temporal extrapolation.

4.2.4. Error distribution analysis

This section examines how prediction accuracy varies across different spatial regions of the wind turbine wake. We divided each cross-section into two key areas: the inner region (within turbine blade radius) where complex vortex patterns dominate, and the outer region where airflow interactions are less complicated. The error is defined as:

$$Error = \frac{u_i - u_i^{pred}}{u_i} \times 100\% \tag{28}$$

where u_i is the velocity obtained by CFD, i.e. the ground truth, and u_i^{pred} is the model prediction.

Fig. 17 shows error plots at four representative downstream locations (4D, 7D, 10D, 14D) at $t = 275$s. The first column is the CFD results (ground truth), while the next three columns show prediction errors for each model, i.e. *wakeEvoNet*-1, *wakeEvoNet*-2, and *wakeEvoNet*-3, respectively. White dotted circles mark the turbine's blade rotation area, separating inner and outer zones.

Table 2 shows the R^2 values of the predictions in the inner and outer

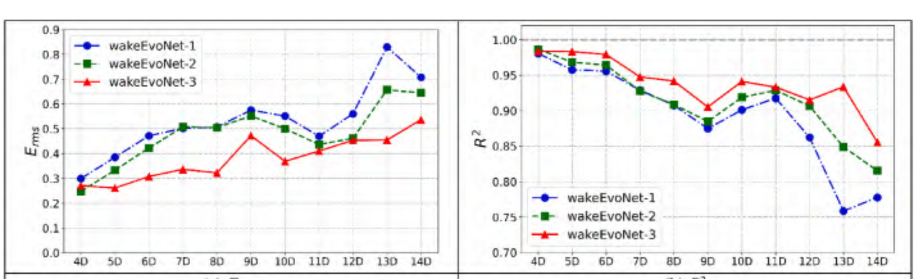

Fig. 14. E_{RMS} & R^2 change with downstream distance.

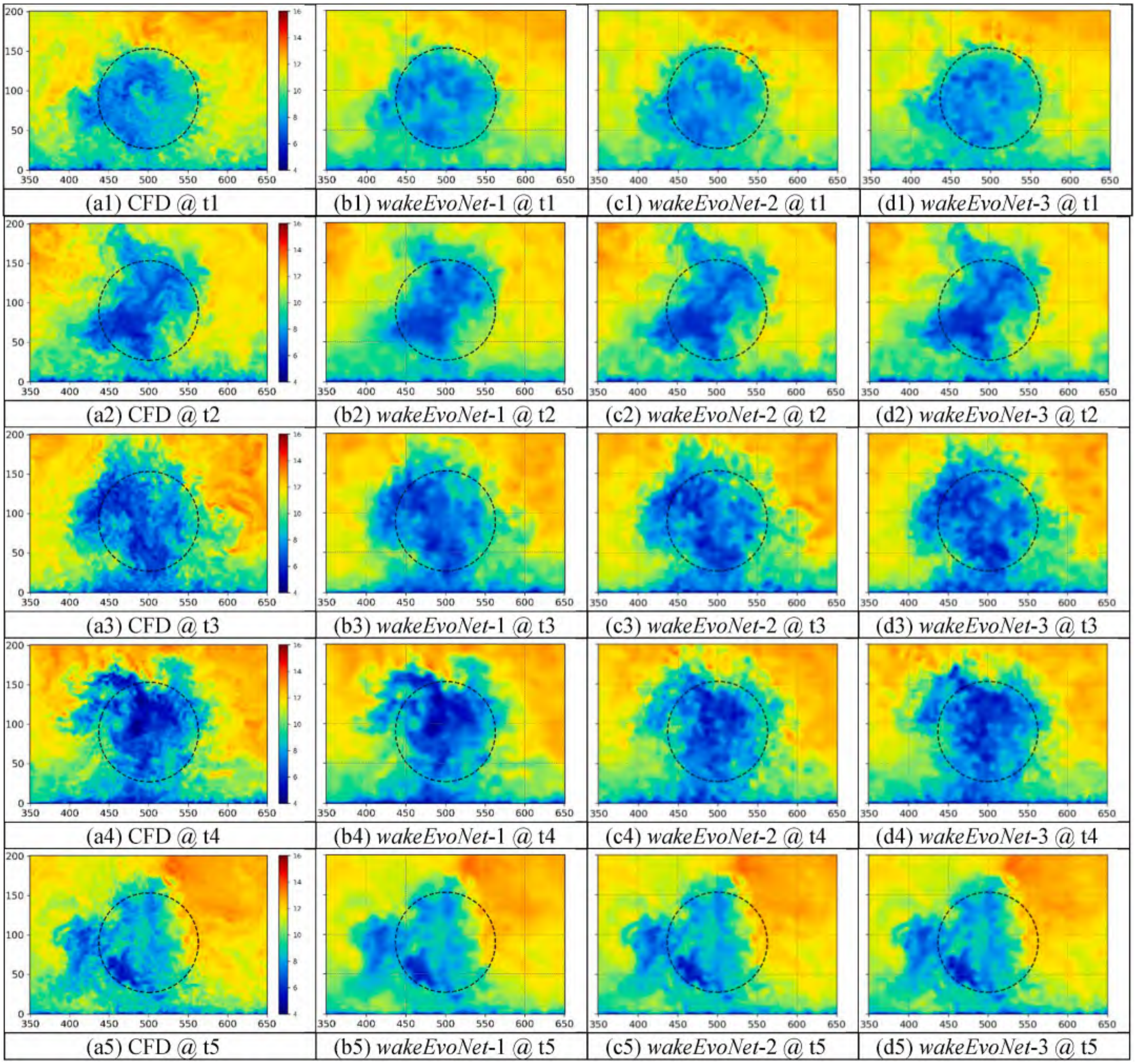

Fig. 15. Comparison of different models at different time instances.

regions at different downstream locations. The data in Table 2 is further visualized by Fig. 18. As depicted in Fig. 18, two groups of bar charts exist: the left group shows the R^2 values within the inner wake region of the predictions obtained by all the three NN models, while the right group correspondingly presents outer-region R^2 values. Systematic analysis reveals these critical observations.

- All models performed better in outer regions (average R^2 advantage: $+0.12$) where wake charactersitics are more predictable. The inner region's complex swirling flow presented greater challenges for all the three NN models.
- The new model proposed in the current study, i.e. *wakeEvoNet*-3, showed remarkable improvement in the critical inner region, e.g., achieving up to 23% higher accuracy than *wakeEvoNet*-1 at 10D. This enhancement comes from the Turbulence Attention (TA) mechanism's ability to focus on important flow features within the swirling wake region. Fig. 18 visually confirms this advantage, showing significantly smaller errors in *wakeEvoNet*-3's center regions beyond downstream distance of 7D.

These findings demonstrate that our TA mechanism can effectively address the core computational bottlenecks in wake prediction. By efficiently extracting complex flow features, TA delivers physics-aware accuracy enhancements in regimes where conventional U-Net architectures often struggle.

4.2.5. Summary

This section summarizes key findings from our comprehensive evaluation of *wakeEvoNet*'s predictive capabilities across spatial, temporal, and regional dimensions. The hybrid physics-data framework demonstrates robust performance in predicting wind turbine wake evolution from 4D to 14D downstream, achieving the core objective of

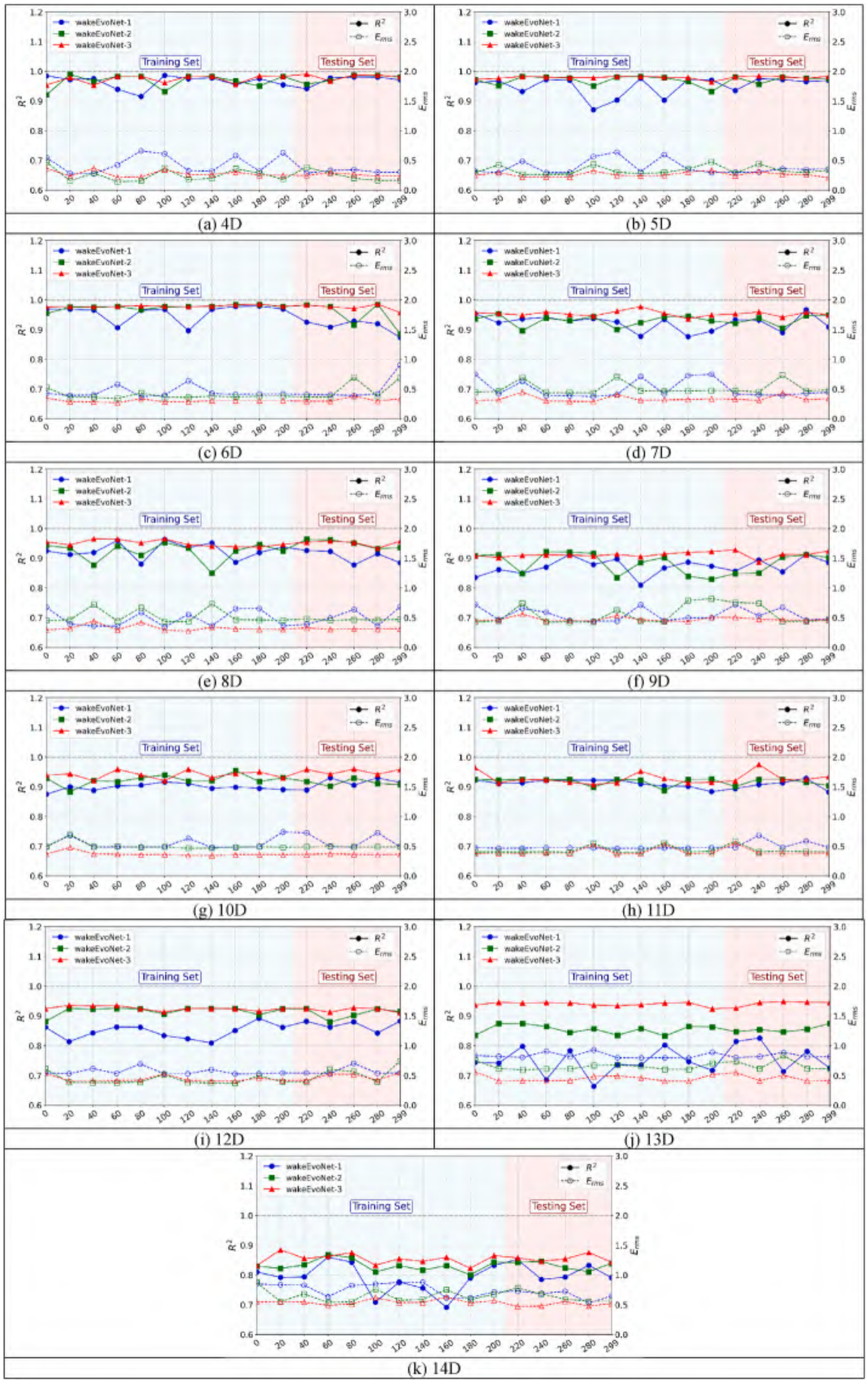

Fig. 16. Temporal accuracy of different models at different downstream locations.

maintaining high accuracy while enabling computationally efficient far-wake forecasting.

Spatially, prediction accuracy exhibits a characteristic yet well-constrained degradation with increasing downstream distance, as shown in Fig. 14. This expected pattern stems fundamentally from error accumulation inherent in rolling predictions. Despite this challenge, *wakeEvoNet*-3 maintains remarkably high accuracy throughout the domain, preserving $R^2 > 0.85$ at all positions (minimum 0.855 at 14D). Temporally, all three models demonstrate satisfactory stability throughout the testing period, with no significant degradation observed across the 300-s duration (Fig. 16). This temporal robustness confirms the effectiveness of the current hybrid physics-data approach in mitigating temporal error accumulation – a critical limitation for purely data-driven models. Regionally, analysis reveals predictable spatial distribution of prediction errors: outer wake regions consistently achieve higher accuracy (mean $R^2 = 0.94$) due to less complex flow physics, while inner regions present greater challenges (mean $R^2 = 0.85$) owing to complex blade-vortex interactions.

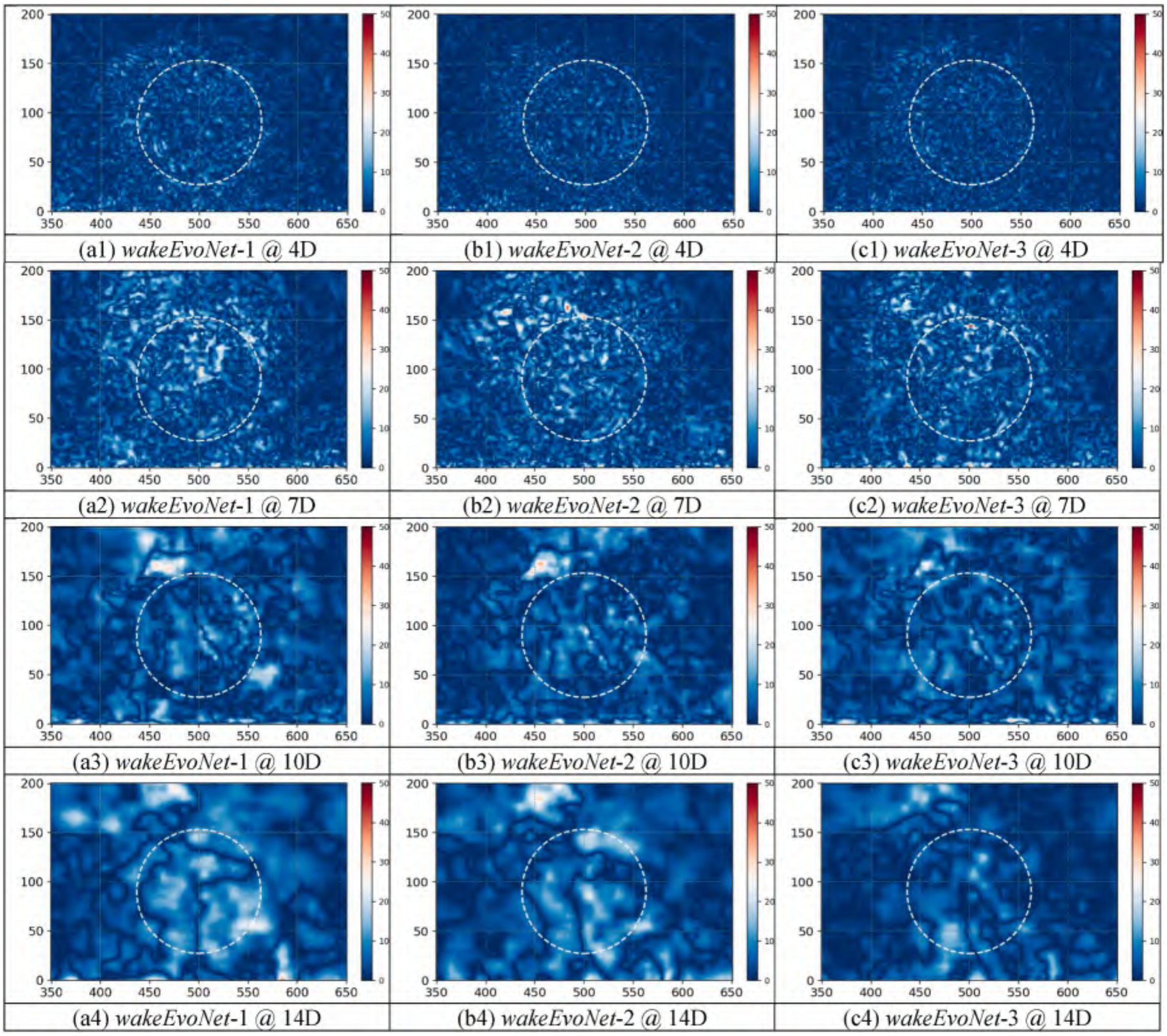

Fig. 17. Error distribution of different models.

Table 2
R^2 values of different regions at different downstream locations obtained by different models.

	wakeEvoNet-1		*wakeEvoNet*-2		*wakeEvoNet*-3	
	Inner	Outer	Inner	Outer	Inner	Outer
4D	0.9570	0.9892	0.9796	0.9951	0.9813	0.9954
5D	0.9493	0.9864	0.9576	0.9896	0.9733	0.9928
6D	0.9488	0.9859	0.9588	0.9870	0.9700	0.9898
7D	0.9378	0.9718	0.9437	0.9769	0.9461	0.9827
8D	0.9078	0.9518	0.9091	0.9611	0.9487	0.9753
9D	0.8592	0.9087	0.8615	0.9032	0.9005	0.9363
10D	0.8897	0.9235	0.9076	0.9398	0.9329	0.9519
11D	0.9005	0.9343	0.9030	0.9403	0.9222	0.9500
12D	0.8254	0.8810	0.8948	0.9228	0.9067	0.9344
13D	0.7084	0.7778	0.8361	0.8855	0.8999	0.9776
14D	0.7232	0.7930	0.8082	0.8645	0.8317	0.9051

4.3. *An input-space latency analysis*

The comprehensive model evaluation presented in the preceding sections clearly indicates that the integration of attention mechanisms has substantially enhanced the predictive capabilities of the neural networks. To elucidate the underlying mechanisms through which these improvements are achieved, this section conducts an input-space latency analysis—also termed sensitivity analysis—which aims to interrogate what the models, and specifically the attention modules, have effectively learned. This methodology evaluates the relative contributions of different regions within the input channels, i.e., the cross-sectional flow fields, to the accuracy of the final prediction by quantifying the gradients with respect to the input features. Regions associated with larger gradients are identified as more critical to model performance, thereby allowing us to approximate which parts of the input feature maps the models prioritize during wake evolution forecasting. The results of this analysis for predictions at 4D and 9D downstream locations are illustrated in Figs. 19 and 20, where the models respectively utilize input from the 1D - 3D and 6D - 8D cross-sections to generate the target outputs.

For clarity in comparison, the sensitivity metrics are normalized across all downstream locations. In these figures, the first row displays the raw input flow fields, followed by the latency maps of *wakeEvoNet*-1 (U-Net), *wakeEvoNet*-2 (CBAM-UNet), and *wakeEvoNet*-3 (CA-TA-UNet) in the subsequent rows, with each column corresponding to one of the three input channels required for the prediction. Notably, darker hues in the latency maps signify areas of higher latency, implying that the models' predictions exhibit greater sensitivity to variations in these regions, thus highlighting the focal points that dominantly influence the wake prediction outcomes.

The input-space latency analysis, as illustrated in Figs. 19 and 20, provides critical insights into the feature prioritization mechanisms of the different *wakeEvoNet* variants. For *wakeEvoNet*-1 (U-Net), the latency

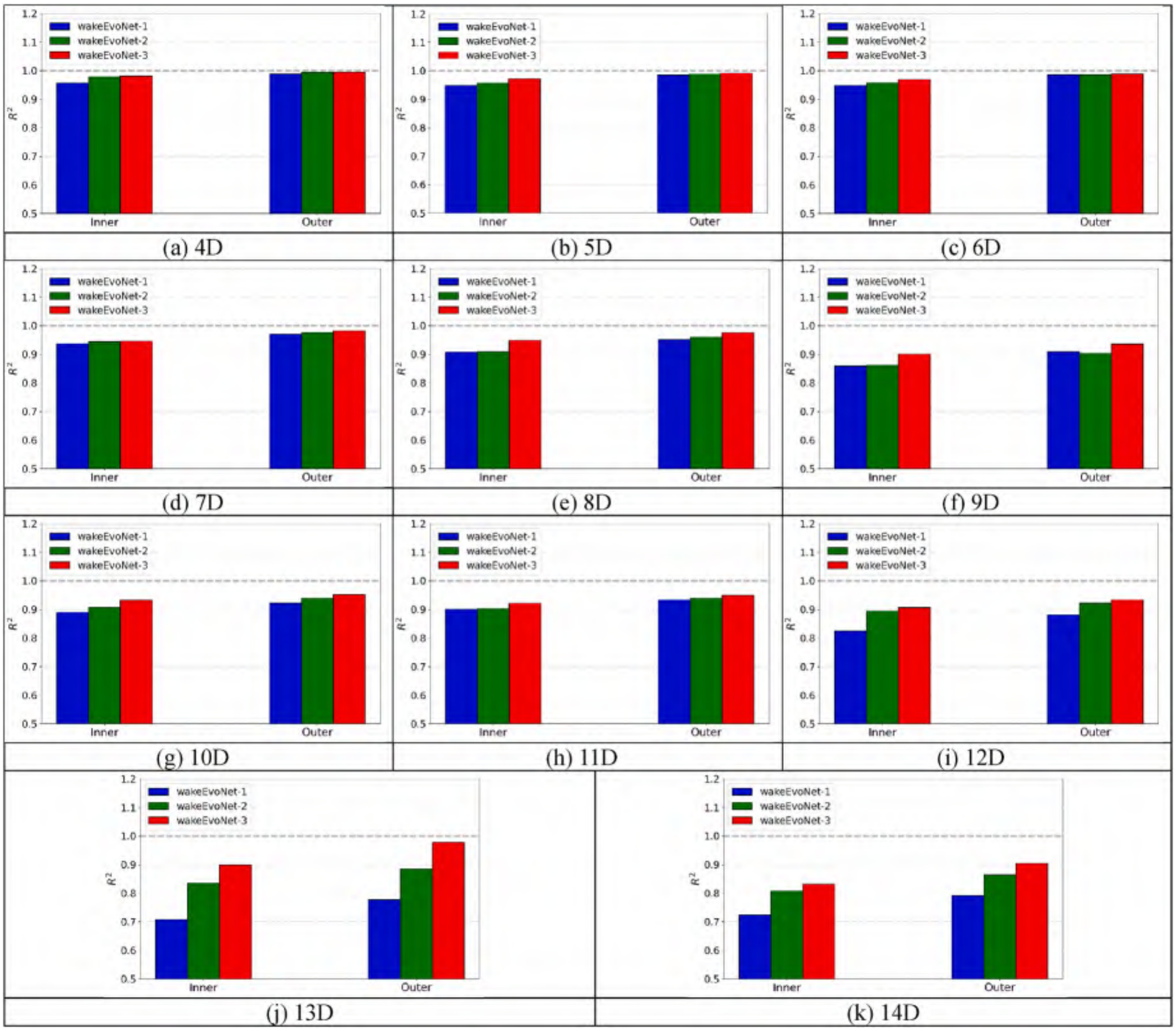

Fig. 18. Comparison of Inner and Outer accuracy of NN predictions.

maps reveal that the region within the wind turbine wake, denoted by the white dotted circle, exhibits darker hues, indicating that the model attributes greater importance to input variations inside the wake area for final predictions, aligning with physical expectations. However, the entire map is generally dark, suggesting that the U-Net model cannot distinctly differentiate between the wake interior and exterior, making it more susceptible to fluctuations in the outer flow field. In contrast, *wakeEvoNet*-2 (CBAM-UNet) shows a clear disparity between the wake interior and exterior in the latency maps, with the outer region appearing significantly lighter, demonstrating that the CBAM attention mechanism suppresses feature contributions from outside the wake and concentrates attention inwardly. Furthermore, *wakeEvoNet*-3 (CA-TA-UNet) exhibits an even more pronounced contrast, where the outer region becomes notably lighter, highlighting that the TA attention mechanism effectively ameliorates the influence of outer flow fields, thereby enhancing the model's ability to focus on critical wake features and improving robustness by reducing sensitivity to peripheral fluctuations.

5. Conclusions

This study developed and validated *wakeEvoNet*, a novel hybrid physics-data driven framework designed to overcome the persistent trade-off between computational cost and prediction accuracy in wind turbine wake forecasting. The core innovation lies in a strategic spatial-decomposition approach: high-fidelity measurements or simulations are confined to the physically complex near-wake region (1D-3D downstream), while computationally efficient neural networks evolve this high-fidelity input to predict the far-wake field (4D-14D downstream). This methodology effectively eliminates the temporal error accumulation inherent in sequential prediction models by re-initializing the prediction chain at each time step with real-time near-wake data.

Three convolutional encoder-decoder architectures were developed and rigorously evaluated. The benchmark U-Net (*wakeEvoNet*-1) established a strong baseline, while the CBAM-enhanced U-Net (*wakeEvoNet*-2) demonstrated improved feature refinement. The most significant advancement was achieved with *wakeEvoNet*-3, which incorporates a novel, physics-guided lightweight Turbine-wake Attention (TA) mechanism. This TA module dynamically weights features based on local velocity characteristics, specifically tailoring the model's focus to the most critical regions of the evolving wake.

Comprehensive evaluations confirmed the framework's robustness. Spatially, while all models exhibited a predictable accuracy decay with downstream distance due to error propagation in the rolling prediction scheme, *wakeEvoNet*-3 consistently outperformed the others, maintaining high accuracy ($R^2 > 0.80$) across the entire domain, with a notable performance advantage of up to 17.5% at 13D compared to the baseline. Temporally, all models demonstrated remarkable stability over the 300-s simulation, with no significant degradation observed, underscoring the effectiveness of the spatial-decomposition strategy in confining temporal errors. Regional error analysis further revealed that *wakeEvoNet*-3 achieved substantial accuracy gains within the challenging inner wake

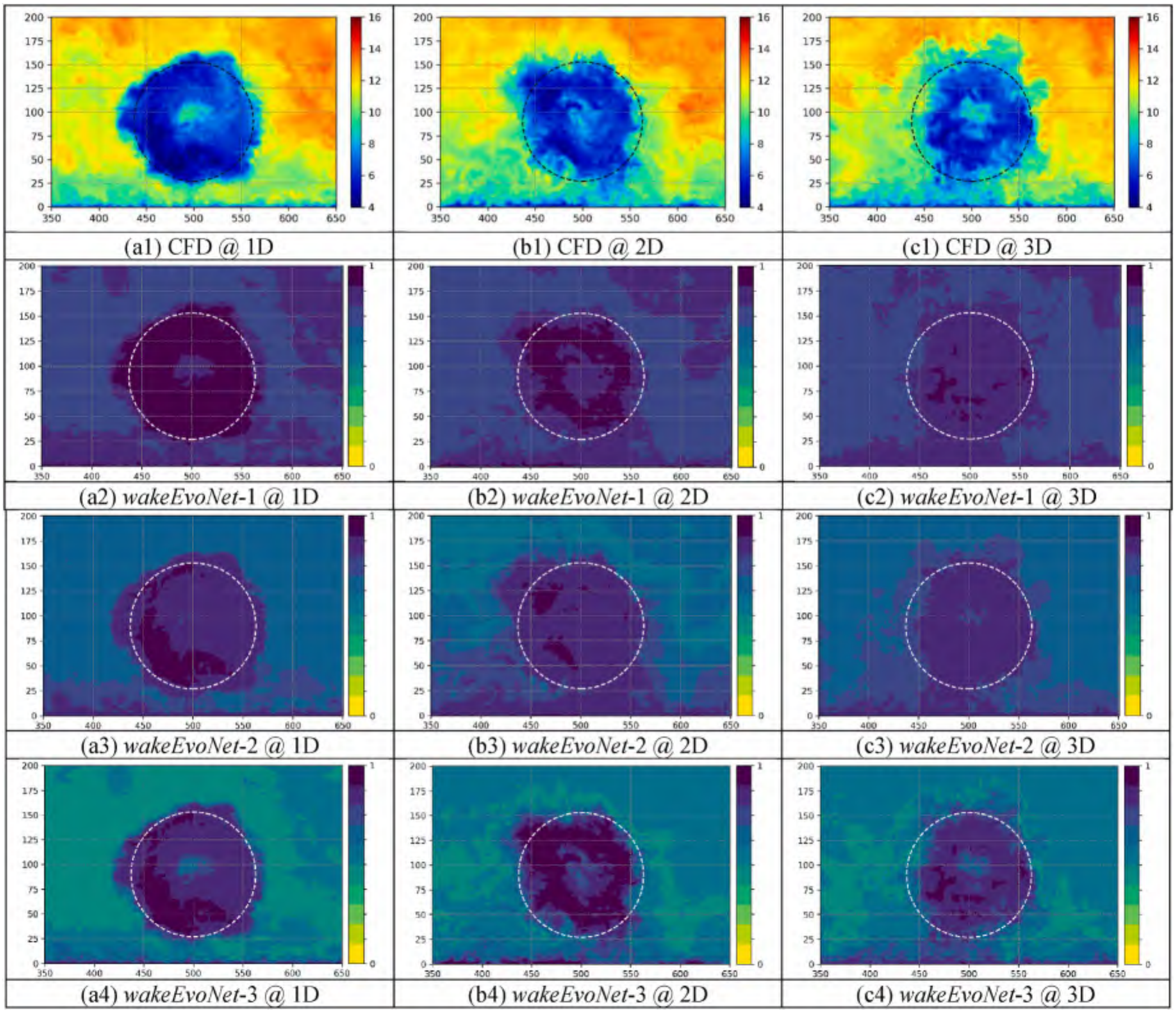

Fig. 19. Heat maps illustrating the latency of the input channels (1D, 2D, and 3D, respectively) in the prediction of the 4D downstream cross-section. Higher latency values correspond to darker colors. Note that all scores for the different channels and models are normalized to the range [0, 1] for comparison. (For interpretation of the references to color in this figure legend, the reader is referred to the Web version of this article.)

region, where complex vortex dynamics dominate. The input-space latency analysis provided critical interpretability, showing that the TA mechanism effectively sharpens the model's focus on the wake interior while suppressing sensitivity to irrelevant fluctuations in the outer flow, thereby enhancing predictive robustness.

The primary contributions of this work are.

- A spatial-decomposition framework that uniquely leverages CFD for near-field physics and neural networks for computationally accelerated far-field evolution, circumventing traditional full-field NN limitations; and
- A physics-guided lightweight spatial attention mechanism, i.e. the turbine-wake attention which adaptively prioritizes high-velocity-magnitude regions to enhance physical fidelity in wind turbine wake modeling.

Key limitations of the current study include.

- Inherent accuracy degradation beyond 9D due to rolling-prediction error accumulation;
- Current work is restricted to fixed prescribed cross-sections rather than arbitrary spatial domains;
- Current work is limited to the wake flow of a fixed wind turbine.

Correspondingly, future work will focus on: (1) incorporating positional embeddings into neural network architectures to enhance model flexibility; (2) investigating framework performance under different inflow conditions; and (3) extending *wakeEvoNet* to floating offshore wind turbines to capture complex unsteady wake dynamics under diverse sea states.

CRediT authorship contribution statement

Maokun Ye: Writing – original draft, Visualization, Validation, Software, Methodology, Investigation, Formal analysis, Data curation. **Hanqiao Han:** Writing – review & editing, Validation, Investigation, Data curation. **Minqiu Liu:** Writing – review & editing, Visualization, Validation, Investigation, Formal analysis, Data curation. **Decheng Wan:** Writing – review & editing, Supervision, Software, Resources, Project administration, Investigation, Funding acquisition, Conceptualization. **Moustafa Abdel-Maksoud:** Writing – review & editing, Validation, Investigation, Data curation.

Declaration of competing interest

The authors declare that they have no known competing financial interests or personal relationships that could have appeared to influence the work reported in this paper.

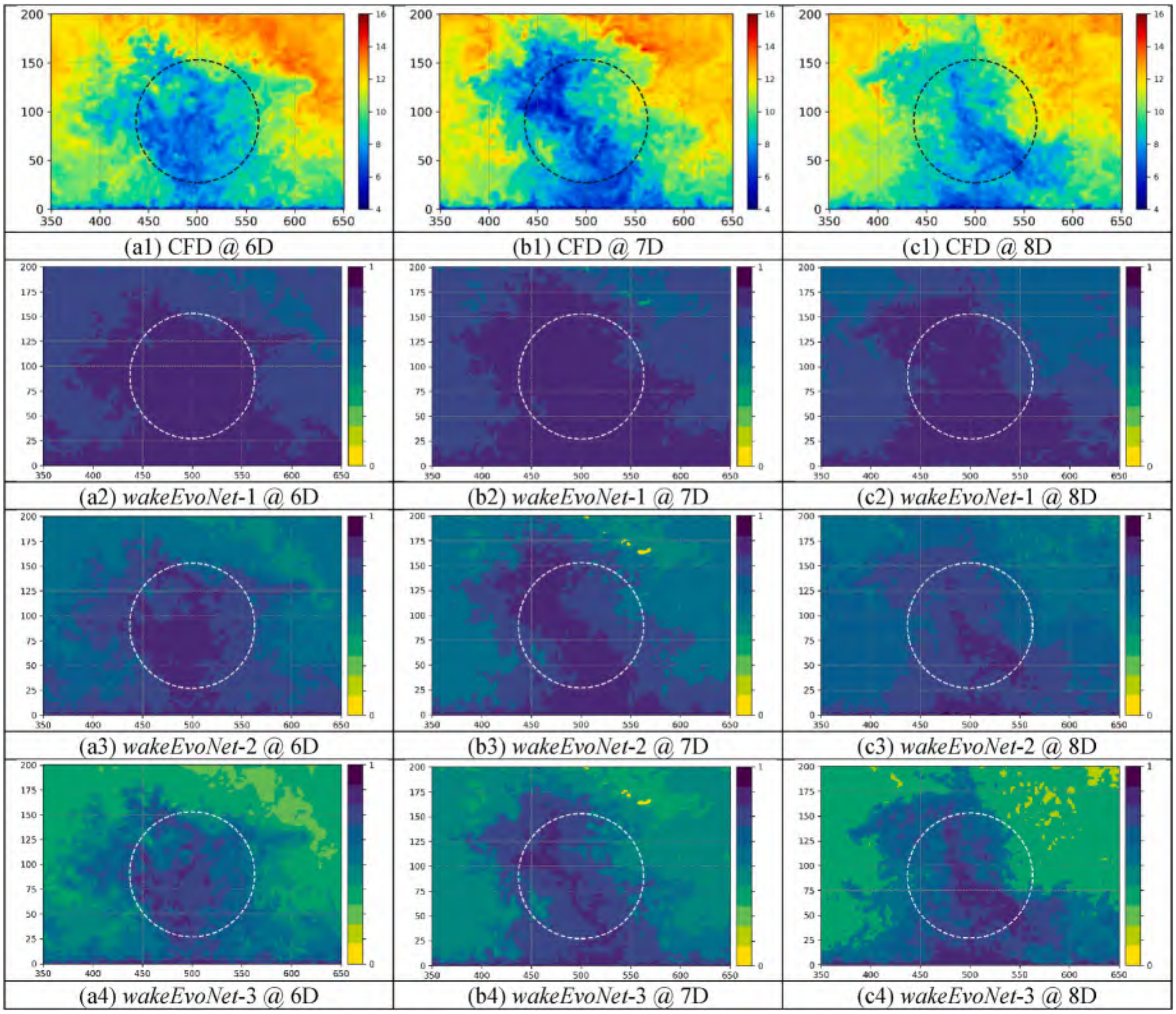

Fig. 20. Heat maps illustrating the latency of the input channels (6D, 7D, and 8D, respectively) in the prediction of the 9D downstream cross-section. Higher latency values correspond to darker colors. Note that all scores for the different channels and models are normalized to the range [0, 1] for comparison. (For interpretation of the references to color in this figure legend, the reader is referred to the Web version of this article.)

Acknowledgements

This work was supported by National Key Research and Development Program of China(2025YFF0519802), and the National Natural Science Foundation of China (52131102), to which the authors are most grateful.

Data availability

The data that support the findings of this study are available from the corresponding author upon reasonable request.

References

Abkar, M., Porté-Agel, F., 2014. Mean and turbulent kinetic energy budgets inside and above very large wind farms under conventionally-neutral condition. Renew. Energy 70, 142–152. https://doi.org/10.1016/j.renene.2014.03.050.

Archer, C.L., et al., 2018. Review and evaluation of wake loss models for wind energy applications. Appl. Energy 226 (May 2018), 1187–1207. https://doi.org/10.1016/j.apenergy.2018.05.085.

Bastankhah, M., Porté-Agel, F., 2014. A new analytical model for wind-turbine wakes. Renew. Energy 70, 116–123. https://doi.org/10.1016/j.renene.2014.01.002.

Brunton, S.L., Noack, B.R., Koumoutsakos, P., 2020. Machine learning for fluid mechanics. Annu. Rev. Fluid Mech. 52, 477–508. https://doi.org/10.1146/annurev-fluid-010719-060214.

Cao, W., Wang, G., Liang, X., Hu, Z., 2024. A STAM-LSTM model for wind power prediction with feature selection. Energy 296, 131030. https://doi.org/10.1016/j.energy.2024.131030.

Chen, Y., et al., 2021. 2-D regional short-term wind speed forecast based on CNN-LSTM deep learning model. Energy Convers. Manag. 244, 114451. https://doi.org/10.1016/j.enconman.2021.114451.

Deng, Z., Chen, Y., Liu, Y., Kim, K.C., 2019. Time-resolved turbulent velocity field reconstruction using a long short-term memory (LSTM)-based artificial intelligence framework. Phys. Fluids 31 (7). https://doi.org/10.1063/1.5111558.

Houtin-Mongrolle, F., Bricteux, L., Benard, P., Lartigue, G., Moureau, V., Reveillon, J., 2020. Actuator line method applied to grid turbulence generation for large-Eddy simulations. J. Turbul. 21 (8), 407–433. https://doi.org/10.1080/14685248.2020.1803495.

Jensen, N.O., 1983. A Note on Wind Generator Interaction, 2411. Risø National Laboratory, Roskilde.

Jonkman, J., Butterfield, S., Musial, W., Scott, G., 2009. Definition of a 5-MW Reference Wind Turbine for Offshore System Development. https://doi.org/10.1002/ajmg.10175.

LeCun, Y., Bengio, Y., 1998. Convolutional networks for images, speech, and time-series. In: The Handbook of Brain Theory and Neural Networks, 1. MIT Press, Cambridge, MA, United States, pp. 255–258.

Lecun, Y., Bengio, Y., Hinton, G., 2015. Deep learning. Nature 521 (7553), 436–444. https://doi.org/10.1038/nature14539.

Lee, S., Churchfield, M., Moriarty, P., Jonkman, J., Michalakes, J., 2012. Atmospheric and wake turbulence impacts on wind turbine fatigue loadings. In: *50th AIAA Aerospace Sciences Meeting Including the New Horizons Forum and Aerospace Exposition*, Nashville, Tennessee. American Institute of Aeronautics and Astronautics. https://doi.org/10.2514/6.2012-540.

Li, S., 2023. End-to-end wind turbine wake modelling with deep graph representation learning. Appl. Energy.

Li, R., Zhang, J., Zhao, X., 2022. Dynamic wind farm wake modeling based on a bilateral convolutional neural network and high-fidelity LES data. Energy 258, 124845.

Li, S., Zhang, M., Piggott, M.D., 2023. End-to-end wind turbine wake modelling with deep graph representation learning. Appl. Energy 339, 120928. https://doi.org/10.1016/j.apenergy.2023.120928.

Li, H., Yang, Q., Li, T., 2024. Wind turbine wake prediction modelling based on transformer-mixed conditional generative adversarial network. Energy 291, 130403. https://doi.org/10.1016/j.energy.2024.130403.

Luo, Z., Wang, L., Xu, J., Wang, Z., Yuan, J., Tan, A.C.C., 2024. A reduced order modeling-based machine learning approach for wind turbine wake flow estimation from sparse sensor measurements. Energy 294, 130772. https://doi.org/10.1016/j.energy.2024.130772.

Lynch, C.E., Smith, M.J., 2013. Unstructured overset incompressible computational fluid dynamics for unsteady wind turbine simulations. Wind Energy 16, 1033–1048. https://doi.org/10.1002/we.

Mikkelsen, R.F., 2003. Actuator disc methods applied to wind turbine. http://orbit.dtu.dk/en/publications/actuator-disc-methods-applied-to-wind-turbines (baf52b7c-f8a4-4073-9925-ee985b59bb00).html.

Moeng, C.-H., 1984. A large-eddy-simulation model for the study of planetary boundary-layer turbulence. J. Atmos. Sci. 41 (13), 2052–2062.

Nilsson, K., et al., 2015. Large-eddy simulations of the lillgrund wind farm. Wind Energy 18, 449–467. https://doi.org/10.1002/we.

Porté-Agel, F., Bastankhah, M., Shamsoddin, S., 2020. Wind-turbine and wind-farm flows: a review. Bound.-Layer Meteorol. 174 (1), 1–59. https://doi.org/10.1007/s10546-019-00473-0.

Qian, G.-W., Ishihara, T., 2018. A new analytical wake model for yawed wind turbines. Energies 11 (3), 665. https://doi.org/10.3390/en11030665.

Ren, S., He, K., Girshick, R., Sun, J., 2017. Faster R-CNN: towards real-time object detection with region proposal networks. IEEE Trans. Pattern Anal. Mach. Intell. 39 (6), 1137–1149. https://doi.org/10.1109/TPAMI.2016.2577031.

Ronneberger, O., Fischer, P., Brox, T., 2015. U-Net: Convolutional Networks for Biomedical Image Segmentation. *arXiv*: arXiv:1505.04597. [Online]. Available: http://arxiv.org/abs/1505.04597. (Accessed 17 October 2024).

Shakoor, R., Hassan, M.Y., Raheem, A., Wu, Y.K., 2016. Wake effect modeling: a review of wind farm layout optimization using Jensen's model. Renew. Sustain. Energy Rev. 58, 1048–1059. https://doi.org/10.1016/j.rser.2015.12.229.

Shao, Z., Wu, Y., Li, L., Han, S., Liu, Y., 2019. Multiple wind turbine wakes modeling considering the faster wake recovery in overlapped wakes. Energies 12 (4). https://doi.org/10.3390/en12040680.

Shen, W.Z., Mikkelsen, R., Sørensen, J.N., Bak, C., 2005. Tip loss corrections for wind turbine computations. Wind Energy (December 2004), 457–475. https://doi.org/10.1002/we.153.

Shen, W.Z., Sørensen, J.N., Zhang, J.H., 2007. Actuator surface model for wind turbine flow computations. In: Eur. Wind Energy Conf. Exhib. 2007 EWEC 2007, 2, pp. 1198–1205.

Shen, W.Z., Zhang, J.H., Sørensen, J.N., 2009. The actuator surface model: a new navier-stokes based model for rotor computations. J. Sol. Energy Eng. Trans. ASME 131 (1), 110021–110029. https://doi.org/10.1115/1.3027502.

Sørensen, J.N., Shen, W.Z., 2002. Numerical modeling of wind turbine wakes. J. Fluid Eng. 124 (June 2002), 393–399. https://doi.org/10.1115/1.1471361.

Stevens, R.J.A.M., Martínez-Tossas, L.A., Meneveau, C., 2018. Comparison of wind farm large eddy simulations using actuator disk and actuator line models with wind tunnel experiments. Renew. Energy 116, 470–478. https://doi.org/10.1016/j.renene.2017.08.072.

Sun, H., Yang, H., 2018. Study on an innovative three-dimensional wind turbine wake model. Appl. Energy 226 (June), 483–493. https://doi.org/10.1016/j.apenergy.2018.06.027.

Ti, Z., Deng, X.W., Yang, H., 2020. Wake modeling of wind turbines using machine learning. Appl. Energy 257 (July 2019), 114025. https://doi.org/10.1016/j.apenergy.2019.114025.

Ti, Z., Deng, X.W., Zhang, M., 2021. Artificial Neural networks based wake model for power prediction of wind farm. Renew. Energy 172, 618–631. https://doi.org/10.1016/j.renene.2021.03.030.

Tran, T.T., Kim, D.H., 2015. The coupled dynamic response computation for a semi-submersible platform of floating offshore wind turbine. J. Wind Eng. Ind. Aerod. 147, 104–119. https://doi.org/10.1016/j.jweia.2015.09.016.

Tran, T.T., Kim, D.H., 2016. A CFD study into the influence of unsteady aerodynamic interference on wind turbine surge motion. Renew. Energy 90, 204–228. https://doi.org/10.1016/j.renene.2015.12.013.

Tran, T., Kim, D., Song, J., 2014. Computational fluid dynamic analysis of a floating offshore wind turbine experiencing platform pitching motion. Energies 7 (8), 5011–5026. https://doi.org/10.3390/en7085011.

Troldborg, N., 2009. Actuator Line Modeling of Wind Turbine Wakes. Technical University of Denmark, Denmark. PhD Thesis.

Veers, P., et al., 2019. Grand challenges in the science of wind energy. Science 366 (6464), eaau2027. https://doi.org/10.1126/science.aau2027.

Woo, S., Park, J., Lee, J.-Y., Kweon, I.S., 2018. CBAM: Convolutional Block Attention Module. https://doi.org/10.48550/arXiv.1807.06521. *arXiv*: arXiv:1807.06521.

Xu, S., Wang, N., Wan, D., Strijhak, S., 2022a. Large eddy simulations for floating wind turbine under complex atmospheric inflow. Proc. Int. Offshore Polar Eng. Conf. 190–197.

Xu, S., Zhao, W., Wan, D., 2022b. Numerical study of dynamic characteristics for offshore wind turbine under complex atmospheric inflow. Lixue XuebaoChinese J. Theor. Appl. Mech. 54 (4), 872–880. https://doi.org/10.6052/0459-1879-21-693.

Xu, S., Zhuang, T., Zhao, W., Wan, D., 2023. Numerical investigation of aerodynamic responses and wake characteristics of a floating offshore wind turbine under atmospheric boundary layer inflows. Ocean. Eng. 279 (April), 114527. https://doi.org/10.1016/j.oceaneng.2023.114527.

Xu, S., Yang, X., Zhao, W., Wan, D., 2024. Numerical analysis of aero-hydrodynamic wake flows of a floating offshore wind turbine subjected to atmospheric turbulence inflows. Ocean. Eng. 300, 117498. https://doi.org/10.1016/j.oceaneng.2024.117498.

Xu, D., Li, Z., Yang, X., Hou, P., Carmo, B., Mao, X., 2026. Data-driven modeling of wind farm wake flow based on multi-scale feature recognition. Renew. Energy 256, 124517. https://doi.org/10.1016/j.renene.2025.124517.

Yang, S., Deng, X., Ti, Z., Yan, B., Yang, Q., 2022. Cooperative yaw control of wind farm using a double-layer machine learning framework. Renew. Energy 193, 519–537. https://doi.org/10.1016/j.renene.2022.04.104.

Ye, M., Chen, H.-C., Koop, A., 2023a. High-fidelity CFD simulations for the wake characteristics of the NTNU BT1 wind turbine. Energy 265 (November 2022), 126285. https://doi.org/10.1016/j.energy.2022.126285.

Ye, M., Chen, H.C., Koop, A., 2023b. Verification and validation of CFD simulations of the NTNU BT1 wind turbine. J. Wind Eng. Ind. Aerod. 234 (February), 105336. https://doi.org/10.1016/j.jweia.2023.105336.

Ye, M., Chen, H.-C., Koop, A., 2024. High-fidelity CFD simulations of two tandemly arrayed wind turbines under various operating conditions. Ocean. Eng. 314, 119703. https://doi.org/10.1016/j.oceaneng.2024.119703.

Ye, M., Zhong, Y., Chen, H.-C., Wan, D., 2026. Investigating the impact of numerical uncertainties in CFD-generated training data on neural network models for wind-turbine wake predictions. Ocean. Eng. 343, 123200. https://doi.org/10.1016/j.oceaneng.2025.123200.

Zhang, J., Zhao, X., 2023. Digital twin of wind farms via physics-informed deep learning. Energy Convers. Manag. 293, 117507. https://doi.org/10.1016/j.enconman.2023.117507.

Zong, H., Porté-Agel, F., 2020. A momentum-conserving wake superposition method for wind farm power prediction. J. Fluid Mech. 889, 1–15. https://doi.org/10.1017/jfm.2020.77.